LETTER

Corrected: Author Correction

https://doi.org/10.1038/s41586-018-0697-7

Autophagy maintains tumour growth through circulating arginine

Laura Poillet-Perez[1], Xiaoqi Xie[1], Le Zhan[1], Yang Yang[1], Daniel W. Sharp[1], Zhixian Sherrie Hu[1], Xiaoyang Su[1,2], Anurag Maganti[1], Cherry Jiang[1], Wenyun Lu[3], Haiyan Zheng[4], Marcus W. Bosenberg[5], Janice M. Mehnert[1,6], Jessie Yanxiang Guo[1,2,7], Edmund Lattime[1,8], Joshua D. Rabinowitz[1,3] & Eileen White[1,9]*

Autophagy captures intracellular components and delivers them to lysosomes, where they are degraded and recycled to sustain metabolism and to enable survival during starvation[1–5]. Acute, whole-body deletion of the essential autophagy gene *Atg7* in adult mice causes a systemic metabolic defect that manifests as starvation intolerance and gradual loss of white adipose tissue, liver glycogen and muscle mass[1]. Cancer cells also benefit from autophagy. Deletion of essential autophagy genes impairs the metabolism, proliferation, survival and malignancy of spontaneous tumours in models of autochthonous cancer[6,7]. Acute, systemic deletion of *Atg7* or acute, systemic expression of a dominant-negative ATG4b in mice induces greater regression of KRAS-driven cancers than does tumour-specific autophagy deletion, which suggests that host autophagy promotes tumour growth[1,8]. Here we show that host-specific deletion of *Atg7* impairs the growth of multiple allografted tumours, although not all tumour lines were sensitive to host autophagy status. Loss of autophagy in the host was associated with a reduction in circulating arginine, and the sensitive tumour cell lines were arginine auxotrophs owing to the lack of expression of the enzyme argininosuccinate synthase 1. Serum proteomic analysis identified the arginine-degrading enzyme arginase I (ARG1) in the circulation of *Atg7*-deficient hosts, and in vivo arginine metabolic tracing demonstrated that serum arginine was degraded to ornithine. ARG1 is predominantly expressed in the liver and can be released from hepatocytes into the circulation. Liver-specific deletion of *Atg7* produced circulating ARG1, and reduced both serum arginine and tumour growth. Deletion of *Atg5* in the host similarly regulated circulating arginine and suppressed tumorigenesis, which demonstrates that this phenotype is specific to autophagy function rather than to deletion of *Atg7*. Dietary supplementation of *Atg7*-deficient hosts with arginine partially restored levels of circulating arginine and tumour growth. Thus, defective autophagy in the host leads to the release of ARG1 from the liver and the degradation of circulating arginine, which is essential for tumour growth; this identifies a metabolic vulnerability of cancer.

To validate whether host autophagy promotes tumour growth, we tested the growth of an autophagy-competent C57Bl/6J isogenic $Braf^{V600E/+}Pten^{-/-}Cdkn2a^{-/-}$ mouse melanoma cell line (termed YUMM 1.1) in C57Bl/6J host mice, without ($Atg7^{+/+}$) and with ($Atg7^{\Delta/\Delta}$) conditional whole-body *Atg7* deficiency (Fig. 1a). YUMM 1.1 tumours were significantly smaller when grown in $Atg7^{\Delta/\Delta}$ hosts compared to $Atg7^{+/+}$ hosts (Fig. 1b), demonstrating that host autophagy promoted tumour growth. The examination of additional cell lines—autophagy-competent isogenic C57Bl/6J $Braf^{V600E/+}Pten^{-/-}Cdkn2a^{-/-}$ YUMM 1.3 melanoma, carcinogen-induced MB49 urothelial carcinoma and $Kras^{G12D/+}p53^{-/-}$ (*p53* is also known as *Trp53*) 71.8 non-small-cell lung cancer cells—revealed a similar requirement for host autophagy for tumour growth (Extended Data Fig. 1a, c, e). The decreased tumour growth observed in $Atg7^{\Delta/\Delta}$ hosts was associated with decreased proliferation. In some tumour types, there was also increased apoptosis (Fig. 1c, Extended Data Fig. 1b, d, f). However, host autophagy was not required for the growth of autophagy-competent isogenic C57Bl/6J $Braf^{V600E/+}Pten^{-/-}Cdkn2a^{-/-}$ YUMM 1.7 and 1.9 melanoma cell lines (Extended Data Fig. 2a–d), which indicates that—although dependency on host autophagy is common—there are tumour-specific adaptation mechanisms.

The melanoma cell lines that are dependent on host autophagy for tumour growth are derived from genetically engineered mouse models of cancer, and therefore have a low mutation burden, low neoantigen load and fail to provoke an efficient T cell response[9]. Nonetheless, autophagy modulates a variety of immune mechanisms that could underlie defective tumour growth in autophagy-deficient hosts. $Atg7^{\Delta/\Delta}$ hosts did not modify infiltration of YUMM 1.1 tumours with $CD3^+$, $CD4^+$ or $CD8^+$ cells (Extended Data Fig. 2e). Depletion of $CD4^+$ and $CD8^+$ T cells modestly increased tumour growth in $Atg7^{+/+}$ hosts but did not significantly rescue growth in $Atg7^{\Delta/\Delta}$ hosts (Extended Data Fig. 2f). Thus, despite the relative increase in the fraction of myeloid-derived suppressor cells and $CD8^+$ T cells in $Atg7^{\Delta/\Delta}$ hosts (Extended Data Fig. 2g), the decreased tumour growth in $Atg7^{\Delta/\Delta}$ hosts was not due to the induction of an anti-tumour T cell response.

Autophagy supports metabolism by recycling cargo to provide anabolic and catabolic substrates[6]. This metabolic recycling function of autophagy promotes mammalian survival during fasting[1–3], and tumour cell survival under conditions of nutrient limitation[4,10,11]. One major source of tumour nutrients is the host blood supply. Accordingly, we tested whether circulating nutrients provided by host autophagy were required for tumour growth. Metabolite profiling of serum from $Atg7^{+/+}$ and $Atg7^{\Delta/\Delta}$ hosts identified 12 metabolites that were decreased and 7 that were increased with autophagy knockout (Fig. 1d, Supplementary Tables 1, 2). Serum arginine was notably downregulated in $Atg7^{\Delta/\Delta}$ compared to $Atg7^{+/+}$ hosts (−2.37 fold change ($\log_2$(serum arginine in $Atg7^{\Delta/\Delta}$/serum arginine in $Atg7^{+/+}$)) (Fig. 1d), confirming previous results[1].

Arginine is a non-essential amino acid derived from the diet, de novo synthesis and protein turnover, and is important for mTOR activation[12], ammonia detoxification through the urea cycle as well as the synthesis of proteins, creatine, polyamines and nitric oxide[13]. It has long been known that some human cancers silence expression of *ASS1*, the gene that encodes argininosuccinate synthase 1 (ASS1), which results in arginine auxotrophy[14]. Without ASS1, cancer cells are unable to synthesize arginine from citrulline and are dependent

[1]Rutgers Cancer Institute of New Jersey, New Brunswick, NJ, USA. [2]Department of Medicine, Robert Wood Johnson Medical School, Rutgers University, New Brunswick, NJ, USA. [3]Department of Chemistry and Lewis-Sigler Institute for Integrative Genomics, Princeton University, Princeton, NJ, USA. [4]Biological Mass Spectrometry Facility, Rutgers University, Robert Wood Johnson Medical School, Rutgers University, Piscataway, NJ, USA. [5]Department of Pathology, Yale University School of Medicine, New Haven, CT, USA. [6]Department of Medicine, Division of Medical Oncology, Developmental Therapeutics Unit, Robert Wood Johnson Medical School, Rutgers University, New Brunswick, NJ, USA. [7]Department of Chemical Biology, Rutgers Ernest Mario School of Pharmacy, Piscataway, NJ, USA. [8]Department of Surgery, Robert Wood Johnson Medical School, Rutgers University, New Brunswick, NJ, USA. [9]Department of Molecular Biology and Biochemistry, Rutgers University, Piscataway, NJ, USA. *e-mail: epwhite@cinj.rutgers.edu

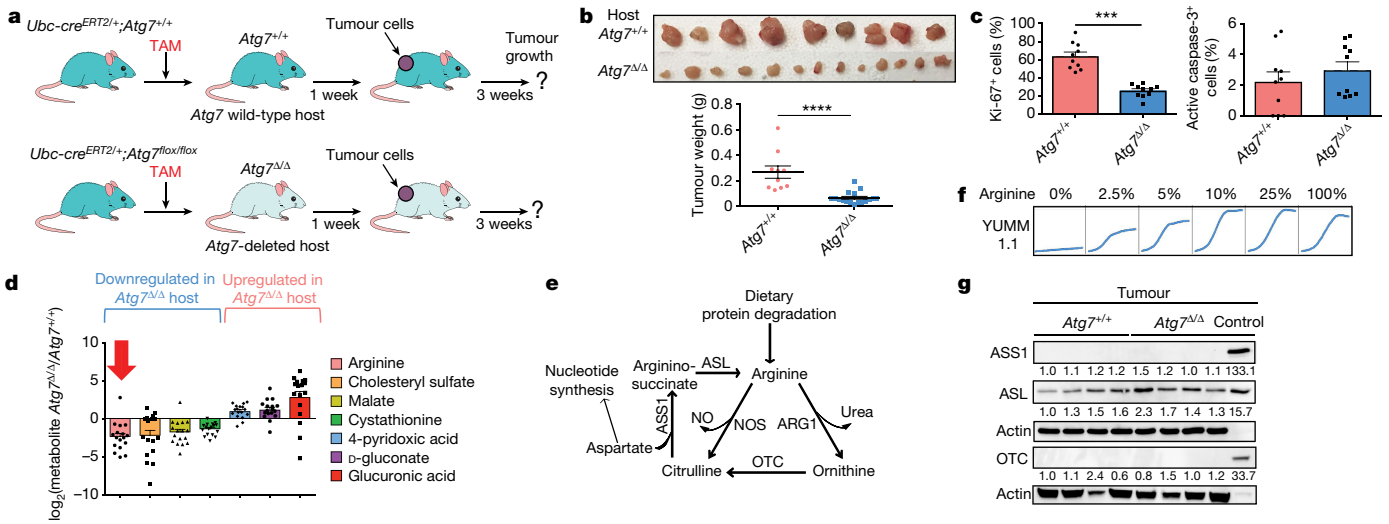

Fig. 1 | Host autophagy promotes growth of arginine auxotrophic tumours. a, Experimental design to induce host mice with conditional whole-body *Atg7* deletion ($Atg7^{\Delta/\Delta}$) and wild-type controls ($Atg7^{+/+}$) with which to assess tumour growth. *Ubc-cre*$^{ERT2/+}$;$Atg7^{+/+}$ and *Ubc-cre*$^{ERT2/+}$;$Atg7^{flox/flox}$ mice were injected with tamoxifen (TAM) to delete *Atg7* and were then injected subcutaneously with tumour cells. Tumour growth was monitored over three weeks. **b**, Comparison of tumour weight between $Atg7^{+/+}$ ($n = 5$) and $Atg7^{\Delta/\Delta}$ ($n = 8$) hosts. Data are mean ± s.e.m. $^{****}P < 0.0001$. **c**, Immunohistochemistry quantification of Ki-67$^+$ and active caspase-3$^+$ cells in tumours from $Atg7^{+/+}$ and $Atg7^{\Delta/\Delta}$ hosts. Data are mean ± s.e.m. $^{***}P < 0.001$. **d**, Serum metabolites with fold-change ($\log_2$(metabolite in $Atg7^{\Delta/\Delta}$/metabolite in $Atg7^{+/+}$)) cut-offs of >1 or <−1 between $Atg7^{+/+}$ ($n = 17$) and $Atg7^{\Delta/\Delta}$ ($n = 17$) hosts obtained by liquid chromatography mass spectrometry (LC–MS), with $P < 0.05$. **e**, Illustration of the arginine metabolism. NO, nitric oxide; NOS, nitric oxide synthetase. **f**, YUMM 1.1 proliferation in vitro, in medium containing different percentages of arginine. Cell density was measured every 2 h using IncuCyte. Data are representative of three independent experiments performed in duplicate. **g**, Western blotting showing expression of ASS1, ASL and OTC in tumours from $Atg7^{+/+}$ and $Atg7^{\Delta/\Delta}$ hosts ($n = 4$ each), representative of three independent experiments. The kidney was used as a control tissue for ASS1 and ASL, and the liver was used for OTC. Actin was used a loading control. In all figures, *n* represents the number of mice.

on exogenous arginine[15,16]. *ASS1* silencing prevents consumption of aspartate by the urea cycle, increasing the availability of this amino acid—which is required for pyrimidine biosynthesis and can become limiting in hypoxia[17,18] (Fig. 1e). These findings suggested that low circulating arginine may underlie defective tumour growth in autophagy-deficient hosts.

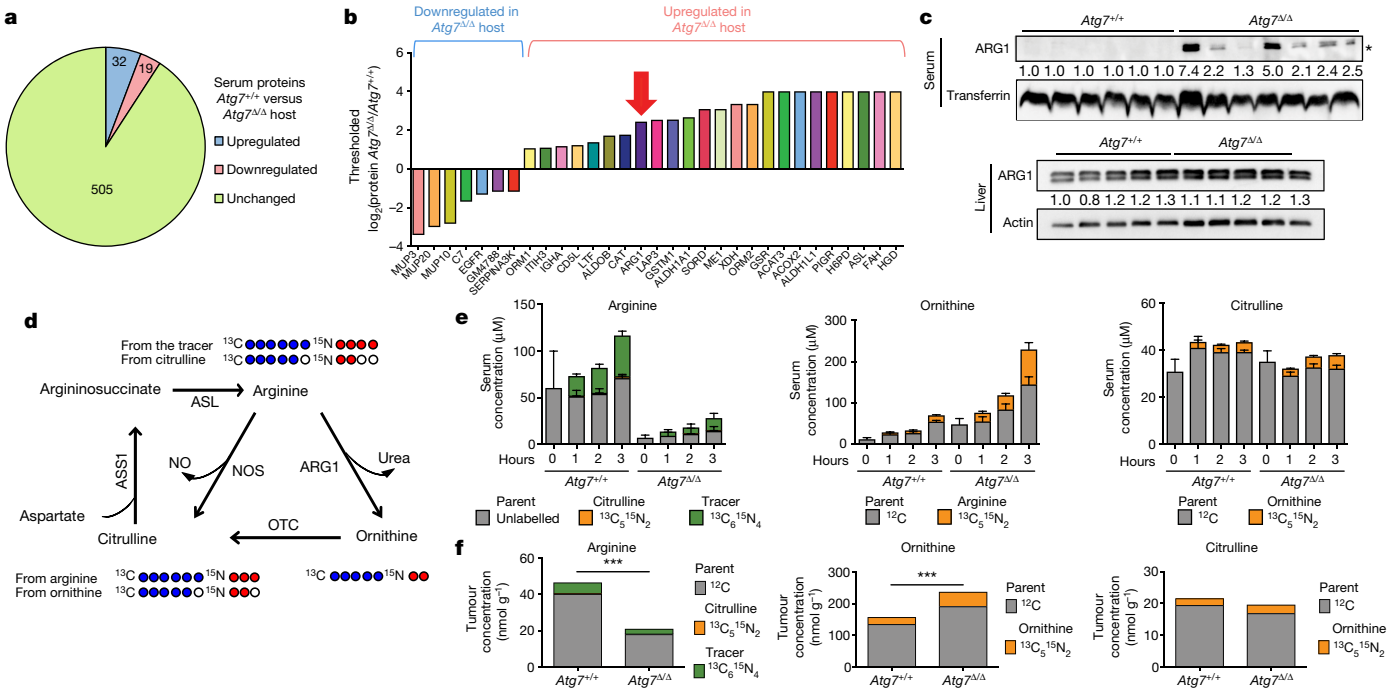

Fig. 2 | Levels of ARG1 in serum increase in $Atg7^{\Delta/\Delta}$ hosts and deplete circulating arginine. a, Comparison of serum proteins between $Atg7^{+/+}$ and $Atg7^{\Delta/\Delta}$ hosts ($n = 5$ each) obtained by nano LC–MS/MS with corrected $P < 0.05$. **b**, Proteins with fold-change ($\log_2$(protein in $Atg7^{\Delta/\Delta}$/protein in $Atg7^{+/+}$)) cut-offs of >1 or <−1 between $Atg7^{+/+}$ and $Atg7^{\Delta/\Delta}$ hosts. **c**, Western blotting showing expression of ARG1 in serum and liver from $Atg7^{+/+}$ and $Atg7^{\Delta/\Delta}$ hosts. $^*P < 0.05$ compared to $Atg7^{+/+}$ hosts. Data are representative of two independent experiments. Actin and transferrin were used as loading controls. **d**, Illustration of the labelling pattern of the $^{13}C_6{}^{15}N_4$ arginine-tracer. **e**, Concentration (in μM) of arginine, citrulline and ornithine in serum from $Atg7^{+/+}$ and $Atg7^{\Delta/\Delta}$ hosts ($n = 3$ and 4, respectively) after infusion with $^{13}C_6{}^{15}N_4$-arginine. Data are mean ± s.e.m. **f**, Concentration (in nmol g^{-1}) of arginine, citrulline and ornithine in tumours from $Atg7^{+/+}$ and $Atg7^{\Delta/\Delta}$ hosts ($n = 2$ each) after infusion with $^{13}C_6{}^{15}N_4$-arginine. Data are mean. $^{***}P < 0.001$ by two-way ANOVA test.

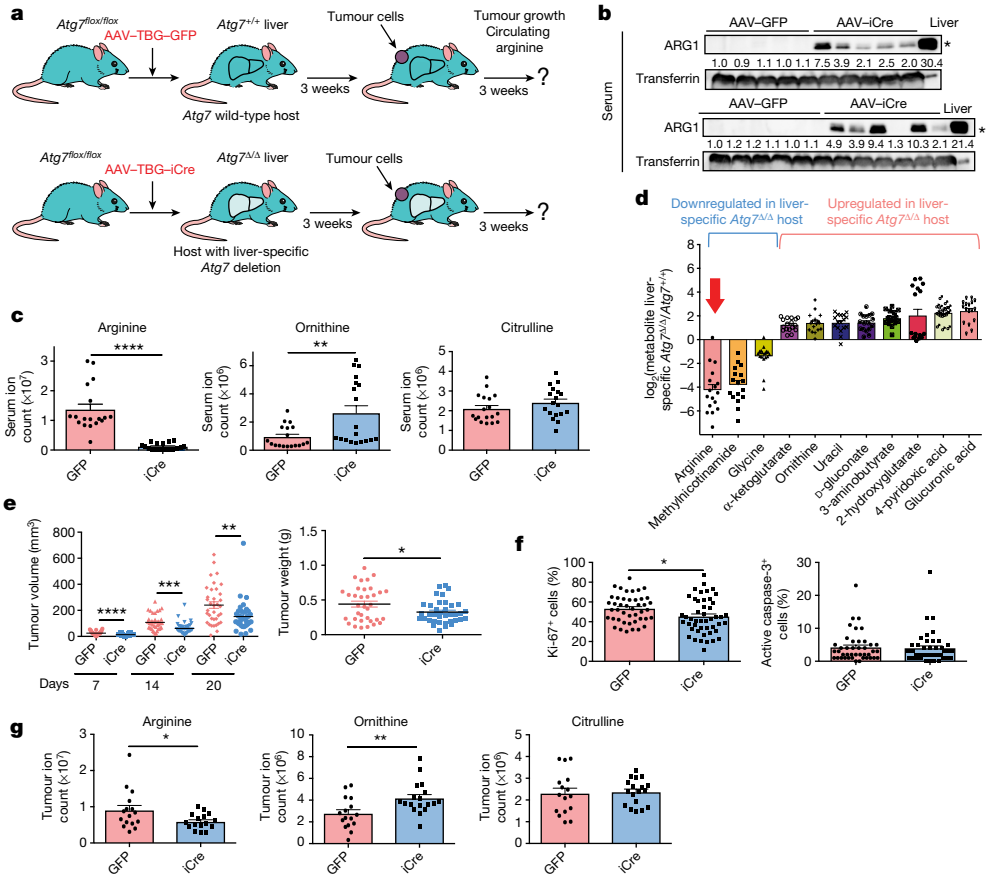

Fig. 3 | *Atg7* deletion in liver increases serum ARG1, and decreases serum arginine and tumour growth. a, Experimental design to induce liver-specific deletion of *Atg7*. $Atg7^{flox/flox}$ mice were injected in the tail vein with AAV–TBG–GFP or AAV–TBG–iCre to delete *Atg7* in the liver, and were injected subcutaneously with tumour cells. Tumour growth was monitored over three weeks. **b**, Western blotting showing expression of ARG1 in serum from $Atg7^{+/+}$ hosts and hosts with liver-specific deletion of *Atg7* ($n = 11$ each). $^*P < 0.05$ compared to $Atg7^{+/+}$ hosts. Data are representative of two independent experiments. Transferrin was used as a loading control. **c**, Levels of arginine, ornithine and citrulline in serum in $Atg7^{+/+}$ hosts and hosts with liver-specific deletion of *Atg7* ($n = 18$ each), obtained by LC–MS. Data are mean ± s.e.m. $^{**}P < 0.01$, $^{****}P < 0.0001$. **d**, Serum metabolites with fold-change ($\log_2$(metabolite in liver-specific $Atg7^{\Delta/\Delta}$/metabolite in $Atg7^{+/+}$)) cut-offs of >1 or <−1 between $Atg7^{+/+}$ hosts and hosts with liver-specific deletion of *Atg7* ($n = 17$ each) obtained by LC–MS, with $P < 0.05$. Data are mean ± s.e.m. **e**, Comparison of tumour volume and weight between $Atg7^{+/+}$ hosts ($n = 17$) and hosts with liver-specific deletion of *Atg7* ($n = 19$). Data are mean ±s.e.m. $^*P < 0.05$, $^{**}P < 0.01$, $^{***}P < <0.001$, $^{****}P < 0.0001$. **f**, Immunohistochemistry quantification of $Ki\text{-}67^+$ and active $caspase\text{-}3^+$ cells in tumours from $Atg7^{+/+}$ and liver-specific $Atg7^{\Delta/\Delta}$ hosts. Data are mean ± s.e.m. $^*P < 0.05$. **g**, Levels of arginine, ornithine and citrulline in tumours in $Atg7^{+/+}$ hosts ($n = 16$) and hosts with liver-specific deletion of *Atg7* ($n = 16$), obtained by LC–MS. Data are mean ± s.e.m. $^*P < 0.05$, $^{**}P < 0.01$.

To determine their requirement for exogenous arginine, YUMM 1.1, 1.3, 1.7, 1.9, MB49 and 71.8 cells were tested for growth without and with arginine. Proliferation was blocked in vitro in complete medium with the sole absence of arginine, and this was not associated with cell death. Growth rates increased with an increased percentage of arginine in the medium, which demonstrates arginine auxotrophy (Fig. 1f, Extended Data Fig. 3a). YUMM 1.1 tumours were tested for the lack of expression of enzymes involved in arginine biosynthesis: ASS1, argininosuccinate lyase (ASL)—which converts citrulline to arginine—and ornithine transcarbamylase (OTC), which converts ornithine to citrulline (Fig. 1e). As previously shown for melanoma[19,20], and irrespective of the use of $Atg7^{+/+}$ and $Atg7^{\Delta/\Delta}$ hosts, tumours lacked ASS1 and OTC expression, which explains their arginine auxotrophy (Fig. 1g). In contrast to tumours, both $Atg7^{+/+}$ and $Atg7^{\Delta/\Delta}$ hosts express ASS1, ASL and OTC in liver and ASS1 and ASL in kidney, which suggests that they are capable of arginine synthesis (Extended Data Fig. 3b). Consistent with findings from the YUMM 1.1 line and the literature[14–16], YUMM 1.7 tumours that grew on $Atg7^{\Delta/\Delta}$ hosts also lacked expression of ASS1 and OTC, which suggests that—in a subset of tumour cell lines—there is a mechanism of intrinsic resistance that is independent of arginine auxotrophy (Extended Data Fig. 3c).

To determine how circulating arginine is depleted in $Atg7^{\Delta/\Delta}$ hosts, we examined the serum proteome by nanoscale liquid chromatography coupled to tandem mass spectrometry (nano LC–MS/MS), which identified 19 proteins that were downregulated and 32 that were upregulated upon loss of *Atg7* (Fig. 2a, Supplementary Table 3). ARG1 was among the proteins that were upregulated in the serum of $Atg7^{\Delta/\Delta}$ hosts (2.43 fold change ($\log_2$(ARG1 in $Atg7^{\Delta/\Delta}$/ARG1 in $Atg7^{+/+}$)) (Fig. 2b). ARG1 is expressed in the liver, where it degrades arginine to ornithine. The appearance of ARG1 in serum, without altered levels in the liver, in $Atg7^{\Delta/\Delta}$ hosts was confirmed by western blotting (Fig. 2c). Levels of nitric oxide in serum were not modified, which suggests that serum ARG1 did not alter the arginine availability for nitric oxide synthesis (Extended Data Fig. 3d). Serum ARG1 activity in vitro was increased, as shown by greater rates of degradation of $^{13}C_6$-arginine to $^{13}C_5$-ornithine in serum from $Atg7^{\Delta/\Delta}$ hosts (Extended Data Fig. 4a). To determine how *Atg7* deficiency altered arginine metabolism in vivo, we infused $Atg7^{+/+}$ and $Atg7^{\Delta/\Delta}$ hosts with $^{13}C_6{}^{15}N_4$-labelled arginine, for three hours[21] (Fig. 2d). To analyse ^{13}C and ^{15}N enrichment, serum was collected at different times during infusion, and tumours, kidneys and livers were collected at the end of the three-hour infusion. The serum of $Atg7^{\Delta/\Delta}$ hosts showed decreased arginine (^{12}C, $^{13}C_6{}^{15}N_4$ and $^{13}C_5{}^{15}N_2$) associated with increased ornithine (^{12}C and $^{13}C_5{}^{15}N_2$), which indicates degradation of circulating arginine to ornithine (Fig. 2e, Extended Data Fig. 4b). Kidneys from $Atg7^{\Delta/\Delta}$ hosts showed decreased levels of arginine, with no change in ornithine or citrulline; no difference was

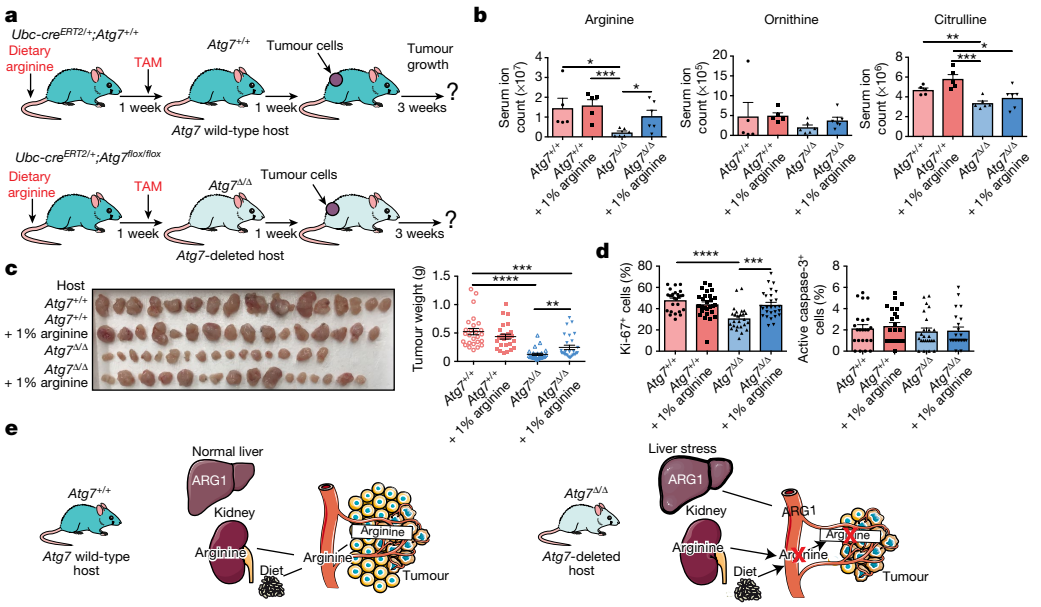

Fig. 4 | Dietary arginine supplementation rescues tumour growth in $Atg7^{\Delta/\Delta}$ hosts. a, Experimental design to perform arginine supplementation and induce conditional whole-body deletion of *Atg7* to assess YUMM 1.1 tumour growth. *Ubc-cre*$^{ERT2/+}$;*Atg7*$^{+/+}$ and *Ubc-cre*$^{ERT2/+}$;*Atg7*$^{flox/flox}$ mice were supplied with supplementary dietary arginine (0 or 1%). Seven days later, tamoxifen was injected to delete *Atg7* and mice were injected subcutaneously with tumour cells. Tumour growth was monitored over three weeks. **b**, Serum arginine, ornithine and citrulline in $Atg7^{+/+}$ ($n = 5$) and $Atg7^{\Delta/\Delta}$ ($n = 6$) hosts with or without arginine supplementation, obtained by LC–MS. Data are mean ± s.e.m. $^*P < 0.05$, $^{**}P < 0.01$, $^{***}P < 0.001$. **c**, Comparison of tumour weight between $Atg7^{+/+}$ ($n = 13$), $Atg7^{+/+}$ + 1% arginine ($n = 13$), $Atg7^{\Delta/\Delta}$ ($n = 13$) and $Atg7^{\Delta/\Delta}$ + 1% arginine ($n = 14$) hosts. Data are mean ± s.e.m. $^{**}P < 0.01$, $^{***}P < < 0.001$, $^{****}P < 0.0001$. **d**, Immunohistochemistry quantification of Ki-67$^+$ and active caspase-3$^+$ cells in tumours from $Atg7^{+/+}$ and $Atg7^{\Delta/\Delta}$ hosts, with or without arginine supplementation. Data are mean ± s.e.m. $^{***}P < 0.001$, $^{****}P < 0.0001$. **e**, Model of host autophagy promoting tumour growth. Illustrations are by Servier (https://smart.servier.com/), CC-BY-3.0.

observed in levels of arginine, citrulline or ornithine in the livers of $Atg7^{\Delta/\Delta}$ hosts compared to $Atg7^{+/+}$ hosts (Extended Data Fig. 4c, d). Tumours from $Atg7^{\Delta/\Delta}$ hosts also displayed decreased levels of arginine (^{12}C, $^{13}C_6{}^{15}N_4$ and $^{13}C_5{}^{15}N_2$) and increased levels of ornithine (^{12}C and $^{13}C_5{}^{15}N_2$) (Fig. 2f). These results confirm that arginine is depleted in ASS1-deficient tumours that are dependent on exogenous arginine, which is consistent with insufficient circulating arginine in $Atg7^{\Delta/\Delta}$ hosts.

During inflammation, injury and liver disease, ARG1 is released from hepatocytes into circulation, which leads to arginine depletion[22]. $Atg7^{\Delta/\Delta}$ hosts have steatosis[1], and liver-specific deletion of *Atg5* or *Atg7* is associated with liver damage[2,23,24]. Accordingly, we hypothesized that ARG1 is released into circulation after deletion of *Atg7* in the liver. To test this hypothesis, we deleted *Atg7* specifically in the liver and examined levels of arginine and ARG1 in circulation, and tumour growth (Fig. 3a). Injection of an AAV–TBG–iCre vector efficiently deleted *Atg7* in the liver, but not in other organs such as the brain and kidney (Extended Data Fig. 5a–c). As expected, liver-specific deletion of *Atg7* led to histopathologic changes in liver cells without affecting other tissues (Extended Data Fig. 5d). As seen in $Atg7^{\Delta/\Delta}$ hosts, serum from hosts with liver-specific deletion of *Atg7* showed increased levels of ARG1 (Fig. 3b), a reduced level of arginine, an increased level of ornithine (Fig. 3c) and no change in the level of nitric oxide (Extended Data Fig. 5e). Liver-specific deletion of *Atg7* also modified levels of other circulating metabolites, with 18 increased and 4 decreased compared to $Atg7^{+/+}$ hosts (Supplementary Tables 4, 5). Some of these circulating metabolites (for example, 4-pyridoxic acid, D-gluconate and glucuronic acid) were also altered in $Atg7^{\Delta/\Delta}$ hosts, which suggests that the dysregulation of these metabolites has a liver-specific origin (Fig. 1d, Extended Data Fig. 5f). The level of arginine in serum was downregulated in hosts with liver-specific deletion of *Atg7* compared to $Atg7^{+/+}$ hosts (Fig. 3d), as was shown in $Atg7^{\Delta/\Delta}$ hosts (Fig. 1d). The weight and volume of YUMM 1.1 melanoma tumours were significantly decreased in hosts with liver-specific deletion of *Atg7*, compared to $Atg7^{+/+}$ hosts (Fig. 3e); this decrease in weight and volume was associated with decreased proliferation and no change in apoptosis (Fig. 3f). Tumours from hosts with liver-specific deletion of *Atg7* had decreased levels of arginine and increased levels of ornithine, but to a lesser extent than the tumours from $Atg7^{\Delta/\Delta}$ hosts—this may explain why the decreased tumour growth in hosts with liver-specific deletion of *Atg7* was not as marked as with $Atg7^{\Delta/\Delta}$ hosts (Fig. 3g). In hosts with liver-specific deletion of *Atg7*, autophagy in the microenvironment may locally feed the tumour with amino acids, as has previously been shown in pancreatic cancer and *Drosophila* tumours[25,26]. These results suggest that deletion of *Atg7* in the liver is responsible for ARG1 release into the circulation, which leads to depletion of circulating arginine and decreased tumour growth.

To determine whether the degradation of circulating arginine by ARG1 in $Atg7^{\Delta/\Delta}$ hosts was due to loss of autophagy, we examined mice with conditional deletion of *Atg5*. Whole-body conditional deletion of *Atg5* also introduced ARG1 into circulation and decreased the level of arginine in serum; tumour growth was also decreased in these $Atg5^{\Delta/\Delta}$ hosts (Extended Data Fig. 6). Similar to liver-specific deletion of *Atg7*, liver-specific deletion of *Atg5* led to histopathologic changes in the liver with increased circulating ARG1 and reduced arginine (Extended Data Fig. 7), which confirms that the modulation of circulating arginine and tumorigenesis was dependent on autophagy.

We next tested whether dietary arginine supplementation can rescue tumour growth in $Atg7^{\Delta/\Delta}$ hosts (Fig. 4a). Dietary arginine supplementation was able to partially increase levels of arginine in serum in $Atg7^{\Delta/\Delta}$ hosts, and did not modify levels of ornithine or citrulline (Fig. 4b). This increased circulating arginine promoted growth and proliferation of the YUMM 1.1 and 1.3 melanoma cell lines in $Atg7^{\Delta/\Delta}$ hosts, compared to $Atg7^{+/+}$ hosts (Fig. 4c, d, Extended Data Fig. 8a–c), confirming that limiting circulating arginine can curtail tumour growth.

In summary, autophagy in the liver prevents the release of ARG1 and the degradation of circulating arginine that is important for the growth of arginine-auxotrophic tumours (Fig. 4e). However, some tumour cells that are auxotrophic for arginine in vitro were capable of growth in $Atg7^{\Delta/\Delta}$ hosts, suggesting that adaptation mechanisms exist[27]. Recent

work has demonstrated that autophagy in the local tumour microenvironment can provide amino acids that promote tumour growth[25,26]. Our work demonstrates that host autophagy also sustains a circulating amino acid—arginine—that is essential for tumour growth. This finding underscores the importance of understanding the sensitivity of ASS1-deficient tumours to arginine deprivation therapy[28], with or without autophagy inhibition[29]. As tumour nutrients are mainly derived from host circulation, restricting essential tumour nutrients in the circulation—as done with asparaginase treatment—is a form of cancer therapy that is ripe for further exploitation[30].

Online content

Any methods, additional references, Nature Research reporting summaries, source data, statements of data availability and associated accession codes are available at https://doi.org/10.1038/s41586-018-0697-7.

Received: 3 May 2018; Accepted: 17 September 2018;
Published online 14 November 2018.

1. Karsli-Uzunbas, G. et al. Autophagy is required for glucose homeostasis and lung tumor maintenance. *Cancer Discov.* **4**, 914–927 (2014).
2. Komatsu, M. et al. Impairment of starvation-induced and constitutive autophagy in *Atg7*-deficient mice. *J. Cell Biol.* **169**, 425–434 (2005).
3. Kuma, A. et al. The role of autophagy during the early neonatal starvation period. *Nature* **432**, 1032–1036 (2004).
4. Guo, J. Y. et al. Autophagy provides metabolic substrates to maintain energy charge and nucleotide pools in Ras-driven lung cancer cells. *Genes Dev.* **30**, 1704–1717 (2016).
5. Kamada, Y., Sekito, T. & Ohsumi, Y. Autophagy in yeast: a TOR-mediated response to nutrient starvation. *Curr. Top. Microbiol. Immunol.* **279**, 73–84 (2004).
6. Kimmelman, A. C. & White, E. Autophagy and tumor metabolism. *Cell Metab.* **25**, 1037–1043 (2017).
7. Amaravadi, R., Kimmelman, A. C. & White, E. Recent insights into the function of autophagy in cancer. *Genes Dev.* **30**, 1913–1930 (2016).
8. Yang, A. et al. Autophagy sustains pancreatic cancer growth through both cell-autonomous and nonautonomous mechanisms. *Cancer Discov.* **8**, 276–287 (2018).
9. Wang, J. et al. UV-induced somatic mutations elicit a functional T cell response in the YUMMER1.7 mouse melanoma model. *Pigment Cell Melanoma Res.* **30**, 428–435 (2017).
10. Strohecker, A. M. et al. Autophagy sustains mitochondrial glutamine metabolism and growth of $Braf^{V600E}$-driven lung tumors. *Cancer Discov.* **3**, 1272–1285 (2013).
11. Guo, J. Y. et al. Autophagy suppresses progression of K-ras-induced lung tumors to oncocytomas and maintains lipid homeostasis. *Genes Dev.* **27**, 1447–1461 (2013).
12. Chantranupong, L. et al. The CASTOR proteins are arginine sensors for the mTORC1 Pathway. *Cell* **165**, 153–164 (2016).
13. Morris, S. M. Jr. Arginine metabolism: boundaries of our knowledge. *J. Nutr.* **137**, 1602S–1609S (2007).
14. Delage, B. et al. Arginine deprivation and argininosuccinate synthetase expression in the treatment of cancer. *Int. J. Cancer* **126**, 2762–2772 (2010).
15. Dillon, B. J. et al. Incidence and distribution of argininosuccinate synthetase deficiency in human cancers: a method for identifying cancers sensitive to arginine deprivation. *Cancer* **100**, 826–833 (2004).
16. Patil, M. D., Bhaumik, J., Babykutty, S., Banerjee, U. C. & Fukumura, D. Arginine dependence of tumor cells: targeting a chink in cancer's armor. *Oncogene* **35**, 4957–4972 (2016).
17. Rabinovich, S. et al. Diversion of aspartate in ASS1-deficient tumours fosters de novo pyrimidine synthesis. *Nature* **527**, 379–383 (2015).
18. Nagamani, S. C. & Erez, A. A metabolic link between the urea cycle and cancer cell proliferation. *Mol. Cell. Oncol.* **3**, e1127314 (2016).
19. Feun, L. G. et al. Negative argininosuccinate synthetase expression in melanoma tumours may predict clinical benefit from arginine-depleting therapy with pegylated arginine deiminase. *Br. J. Cancer* **106**, 1481–1485 (2012).
20. Lam, T. L. et al. Recombinant human arginase inhibits the in vitro and in vivo proliferation of human melanoma by inducing cell cycle arrest and apoptosis. *Pigment Cell Melanoma Res.* **24**, 366–376 (2011).
21. Hui, S. et al. Glucose feeds the TCA cycle via circulating lactate. *Nature* **551**, 115–118 (2017).
22. Morris, S. M. Jr. Arginases and arginine deficiency syndromes. *Curr. Opin. Clin. Nutr. Metab. Care* **15**, 64–70 (2012).
23. Takamura, A. et al. Autophagy-deficient mice develop multiple liver tumors. *Genes Dev.* **25**, 795–800 (2011).
24. Komatsu, M. et al. Homeostatic levels of p62 control cytoplasmic inclusion body formation in autophagy-deficient mice. *Cell* **131**, 1149–1163 (2007).
25. Sousa, C. M. et al. Pancreatic stellate cells support tumour metabolism through autophagic alanine secretion. *Nature* **536**, 479–483 (2016).
26. Katheder, N. S. et al. Microenvironmental autophagy promotes tumour growth. *Nature* **541**, 417–420 (2017).
27. Kremer, J. C. et al. Arginine deprivation inhibits the Warburg effect and upregulates glutamine anaplerosis and serine biosynthesis in ASS1-deficient cancers. *Cell Reports* **18**, 991–1004 (2017).
28. Yau, T. et al. A phase 1 dose-escalating study of pegylated recombinant human arginase 1 (Peg-rhArg1) in patients with advanced hepatocellular carcinoma. *Invest. New Drugs* **31**, 99–107 (2013).
29. Shen, W. et al. A novel and promising therapeutic approach for NSCLC: recombinant human arginase alone or combined with autophagy inhibitor. *Cell Death Dis.* **8**, e2720 (2017).
30. Koprivnikar, J., McCloskey, J. & Faderl, S. Safety, efficacy, and clinical utility of asparaginase in the treatment of adult patients with acute lymphoblastic leukemia. *Onco Targets Ther.* **10**, 1413–1422 (2017).

Acknowledgements This work was supported by National Institutes of Health grants: R01CA130893, R01CA188096 (to E.W.), R01CA163591 (to E.W. and J.D.R.), K22CA190521 (to J.Y.G.), R50CA211437 (to W.L.), R01CA193970 and the V Foundation for Cancer Research (to J.M.M.). L.P.-P. received support from a postdoctoral fellowship from the New Jersey Commission for Cancer Research (DHFS16PPC034). We thank the Rutgers-New Brunswick/Robert Wood Johnson Medical School Biological Mass Spectrometry Facility (S10OD016400) for mass spectrometry analysis, and the Biospecimen Repository and Histopathology Service, Metabolomics Service, Flow Cytometry and Biometrics Shared Resources (D. Moore performed the statistical analysis of the proteomics data) of Rutgers Cancer Institute of New Jersey (P30CA072720).

Reviewer information *Nature* thanks R. DeBerardinis and the other anonymous reviewer(s) for their contribution to the peer review of this work.

Author contributions L.P.-P. performed the majority of the experimental work and wrote the manuscript. L.Z. performed surgery and infusion with labelled arginine. Y.Y. developed the methods and provided the mice required for generating $Atg5^{\Delta/\Delta}$ and hosts with liver-specific deletion of *Atg5*. A.M. and C.J. assisted with in vitro experiments. X.X. and J.Y.G. performed some of the tumour growth experiments. J.M.M. provided melanoma expertise. D.W.S. and E.L. assisted with CD4 and CD8 depletion. Z.S.H. assisted with mouse husbandry. H.Z. performed proteomics processing and analysis. X.S., W.L. and J.D.R. performed metabolomics processing and analysis. M.W.B. provided YUMM 1.1, 1.3, 1.7 and 1.9 melanoma cells. E.W. is the leading principal investigator who conceived the project, supervised research and edited the paper.

Competing interests E.W. is co-founder of Vescor Therapeutics. The other authors declare no competing interests.

Additional information
Extended data is available for this paper at https://doi.org/10.1038/s41586-018-0697-7.
Supplementary information is available for this paper at https://doi.org/10.1038/s41586-018-0697-7.
Reprints and permissions information is available at http://www.nature.com/reprints.
Correspondence and requests for materials should be addressed to E.W.
Publisher's note: Springer Nature remains neutral with regard to jurisdictional claims in published maps and institutional affiliations.

METHODS

Mice. All animal care and treatments were carried out in compliance with Rutgers University Institutional Animal Care and Use Committee guidelines (IACUC). Mice for conditional whole-body deletion of *Atg7* (C57Bl/6J *Ubc-cre*$^{ERT2/+}$;*Atg7*$^{flox/flox}$) were engineered with floxed alleles of *Atg7* (*Atg7*$^{flox/flox}$)[2] and a transgene expressing the TAM-regulated Cre recombinase fusion protein under the control of the ubiquitously expressed ubiquitin C promoter (*Ubc*)[31], as previously described[1]. Acute deletion of *Atg7* throughout the mouse is obtained after TAM injection[1]. TAM (T5648, Sigma) was suspended at a concentration of 20 mg/ml, in a mixture of 98% sunflower seed oil and 2% ethanol and 250 μl per 25 g of body weight was injected intraperitoneally into 8–10-week-old male *Ubc-cre*$^{ERT2/+}$;*Atg7*$^{+/+}$ or *Ubc-cre*$^{ERT2/+}$;*Atg7*$^{flox/flox}$ mice once per day for four days to generate cohorts of *Atg7*-deleted (*Atg7*$^{\Delta/\Delta}$) and wild-type (*Atg7*$^{+/+}$) control host mice. To assess the consequence of acute deletion of *Atg7* on tumorigenesis of C57Bl/6J isogenic male tumour cells, one week after TAM treatment, YUMM 1.1 (1×10^6 cells), 1.3 (2×10^6 cells), 1.7 (0.1×10^6 cells), 1.9 (1×10^6 cells), 71.8 (1×10^6 cells) or MB49 (0.25×10^6 cells) cells were resuspended in 100 μl PBS and injected subcutaneously into the dorsal flanks of mice. Three weeks after cell injection, mice were killed and serum and tumours were collected. The maximal tumour volume (1,700 mm^3) permitted by Rutgers University IACUC was never exceeded. For arginine supplementation, 1% arginine (A8094, Sigma) in drinking water was given to the mice a week before TAM and throughout the experiment.

Mice for conditional whole-body deletion of *Atg5* (C57Bl/6J *Ubc-cre*$^{ERT2/+}$;*Atg5*$^{flox/flox}$) were engineered with floxed alleles of *Atg5* (*Atg5*$^{flox/flox}$)[32] and a transgene expressing the TAM-regulated Cre recombinase fusion protein under the control of the *Ubc* promoter[31]. Acute deletion of *Atg5* throughout mice was obtained after TAM injection (250 μl of TAM per 25 g of body weight injected intraperitoneally into 8–10-week-old male *Ubc-cre*$^{ERT2/+}$;*Atg5*$^{+/+}$ or *Ubc-cre*$^{ERT2/+}$;*Atg5*$^{flox/flox}$ mice once a week for four weeks) to generate cohorts of *Atg5*-deleted (*Atg5*$^{\Delta/\Delta}$) and wild-type (*Atg5*$^{+/+}$) control host mice.

Liver-specific deletion of *Atg7* and *Atg5* was achieved by injecting an adeno-associated virus (AAV)–thyroxine binding globulin (TBG) promoter–Cre recombinase vector (AAV–TBG–iCre, Vector Biolabs) into *Atg7*$^{flox/flox}$ and *Atg5*$^{flox/flox}$ mice. An AAV–TBG promoter–GFP vector (AAV–TBG–GFP, Vector Biolabs) was injected into *Atg7*$^{flox/flox}$ and *Atg5*$^{flox/flox}$ mice as a control. 1.5×10^{11} genome copies of either AAV–TBG–iCre or AAV–TBG–GFP vectors in 100 μl PBS were injected into the tail vein of 8–10-week-old male *Atg7*$^{flox/flox}$ and *Atg5*$^{flox/flox}$ mice to generate liver-specific *Atg7*$^{\Delta/\Delta}$ or *Atg5*$^{\Delta/\Delta}$ and *Atg7*$^{+/+}$ or *Atg5*$^{+/+}$ control mice, respectively. Three weeks post injection, YUMM 1.1 cells (1×10^6 cells) were resuspended in 100 μl PBS and injected subcutaneously into the dorsal flanks of the liver-specific *Atg7*$^{\Delta/\Delta}$ and *Atg7*$^{+/+}$ control mice. Tumour growth was monitored daily. Tumour volume was calculated with the following formula: volume $= \pi/6 \times L \times W \times H$. Three weeks after cell injection, mice were killed and liver, kidney, brain, serum and tumours were collected.

Cell lines. *Cell culture*. Cell lines were authenticated using whole-exome sequencing. YUMM 1.1, 1.3, 1.7 and 1.9 cells derived from *Braf*$^{V600E/+}$*Pten*$^{-/-}$*Cdkn2a*$^{-/-}$ C57Bl/6J mouse melanomas were previously generated[33] and cultured in Dulbecco's minimum essential medium and Ham's F12 (DMEM-F12) (10-092-CV, Corning) supplemented with 10% fetal bovine serum (FBS) (F0926, Sigma) in a 5% CO_2 incubator at 37 °C. The mouse lung cancer cell line 71.8 was previously derived from *p53*$^{-/-}$*Kras*$^{G12D/+}$ mouse lung tumours[11] and the MB49 cell line[34] was provided by the Ratliff laboratory and cultured in Roswell Park Memorial Institute medium (RPMI) (11875-093, Gibco). Cells were tested negative for mycoplasma contamination.

Cell proliferation in arginine-deficient medium. YUMM 1.1, 1.3, 1.7, 1.9, 71.8 and MB49 cells were seeded at a density of 15,000 cells per well in 24-well plates. The following day, cells were washed with phosphate-buffered saline (PBS) (14190-144, Gibco) and cultured in arginine-free DMEM-F12 (DFL27, Caisson Labs) or arginine-free RPMI (R1780, Sigma) supplemented with 10% dialysed FBS (89986, Thermo Scientific) and an increasing percentage of arginine from 2.5 to 100%. Growth was assessed using an IncuCyte ZOOM with images of the proliferative cells recorded every 2 h for a total duration of 6 days.

Metabolite analysis by LC–MS. *Metabolite extraction for LC–MS*. Metabolites from 10-μl serum samples were first extracted with 40 μl of ice-cold methanol. The mixture was allowed to sit at −20 °C for 20 min, and then centrifuged at 16,000*g* for 10 min at 4 °C. Supernatants were transferred to clean tubes and pellets were extracted again with 200 μl 40:40:20 methanol:acetonitrile:H_2O. The mixture was allowed to sit on ice for 10 min, and then centrifuged at 16,000*g* for 10 min at 4 °C. Supernatants were combined with the first extraction, resulting in roughly 240 μl of extract. Extracts were further processed with Phree Phospholipid Removal 1-ml Tube (Phenomenex), according to the manufacturer's instructions. The final extract was stored at −80 °C until analysis by LC–MS. To extract metabolites from the tissues and tumours, samples (25 mg) were first pulverized using a Cryomill (Retsch) in liquid nitrogen at 25 Hz for 2 min. Extraction was performed by adding −20 °C 40:40:20 methanol:acetonitrile:water with 0.5% formic acid solution (500 μl) to the ground samples, followed by vortexing and centrifugation at 16,000*g* for 10 min at 4 °C. The supernatants were transferred to clean tubes and the pellets were extracted again by repeating the previous step. The supernatant was then combined with the first extract. Then, 500 μl of extract was neutralized with 44 μl of 15% NH_4HCO_3 solution and centrifuged at 16,000*g* for 10 min at 4 °C to remove protein precipitate. Then, 300 μl of supernatant was removed to clean tubes and stored at −80 °C until analysis by LC–MS.

LC–MS analysis. LC–MS analysis of the extracted metabolites was performed on a Q Exactive PLUS hybrid quadrupole-orbitrap mass spectrometer (Thermo Fisher Scientific) coupled to hydrophilic interaction chromatography. The LC separation was performed on an UltiMate 3000 UHPLC system with an XBridge BEH Amide column (150 mm × 2.1 mm, 2.5 μM particle size, Waters) with the corresponding XP VanGuard Cartridge. The liquid chromatography used a gradient of solvent A (95%:5% H_2O:acetonitrile with 20 mM ammonium acetate, 20 mM ammonium hydroxide, pH 9.4), and solvent B (20%:80% H_2O:acetonitrile with 20 mM ammonium acetate, 20 mM ammonium hydroxide, pH 9.4). The gradient was 0 min, 100% B; 3 min, 100% B; 3.2 min, 90% B; 6.2 min, 90% B; 6.5 min, 80% B; 10.5 min, 80% B; 10.7 min, 70% B; 13.5 min, 70% B; 13.7 min, 45% B; 16 min, 45% B; 16.5 min, 100% B. The flow rate was 300 μl/min. Injection volume was 5 μl and column temperature 25 °C. The mass spectrometry scans were in negative-ion mode with a resolution of 70,000 at *m*/*z* 200. The automatic gain control target was 3×10^6 and the scan range was 75−1,000. To increase metabolome coverage, the samples were also analysed with a secondary LC–MS method, which involves two separate instrument platforms covering both positively charged and negatively charged metabolites. Negatively charged metabolites were analysed via reverse-phase ion-pairing chromatography coupled to an Exactive orbitrap mass spectrometer (Thermo Fisher Scientific). The mass spectrometer was operated in negative ion mode with resolving power of 100,000 at *m*/*z* 200, scanning range being *m*/*z* 75–1,000. The liquid chromatography method has previously been described[35], using a Synergy Hydro-RP column (100 mm × 2 mm, 2.5 μm particle size, Phenomenex) with a flow rate of 200 μl/min. The liquid chromatography gradient was 0 min, 0% B; 2.5 min, 0% B; 5 min, 20% B; 7.5 min, 20% B; 13 min, 55% B; 15.5 min, 95% B; 18.5 min, 95% B; 19 min, 0% B; 25 min, 0% B. Solvent A is 97:3 water:methanol with 10 mM tributylamine and 15 mM acetic acid; solvent B is methanol. Positively charged metabolites were analysed on a Q Exactive Plus mass spectrometer coupled to Vanquish UHPLC system (Thermo Fisher Scientific). The mass spectrometer was operated in positive-ion mode with resolving power of 140,000 at *m*/*z* 200, scanning range being *m*/*z* 75–1,000. The liquid chromatography separation was achieved on an Agilent Poroshell 120 Bonus-RP column (150 × 2.1 mm, 2.7 μm particle size). The gradient was 0 min, 50 μl/min, 0.0%B; 6 min, 50 μl/min, 0% B; 12 min, 200 μl/min, 70% B; 14 min, 200 μl/min, 100%B; 18 min, 200 μl/min, 100% B; 19 min, 200 μl/min, 0% B; 24 min, 200 μl/min, 0% B; 25 min, 50 μl/min, 0% B. Solvent A is 10 mM ammonium acetate + 0.1% acetic acid in 98:2 water:acetonitrile and solvent B is acetonitrile[36]. Metabolite features were extracted in MAVEN v.707[37] with the labelled isotope specified and a mass accuracy window of 5 p.p.m. For the $^{13}C^{15}N$ arginine infusions, the isotope natural abundance and impurity of labelled substrate was corrected using a matrix-based algorithm.

Labelled arginine infusion. For jugular vein catheterization, the procedure was modified from work previously described[38]. In brief, *Atg7*$^{\Delta/\Delta}$ and *Atg7*$^{+/+}$ mice were anaesthetized using isoflurane carried by oxygen, followed by placement of a central venous catheter (polyurethane tubing, 1 F in OD) (SAI Infusion Technologies) into the right jugular vein. A minimal amount of blood was carefully withdrawn to verify the catheter patency. Afterwards, the saline solution in the catheter was replaced by heparin–glycerol catheter lock solution (SAI Infusion Technologies). The proximal end of the catheter was then tunnelled subcutaneously, exited between the shoulder blades and properly secured. A fully recovered surgical mouse was placed in a plastic harness (SAI Infusion Technologies), and the catheter was connected to an infusion pump (New Era Pump System) through a mouse tether and swivel system (Instech Laboratories). Arginine isotope tracer ($^{13}C_6{}^{15}N_4$, CNLM-539-H-PK, Cambridge Isotope Laboratories) was dissolved in sterile saline and infused at a rate of 3.5 nmol/g/min (0.1 μl/g/min) for 3 h. Infusion rate was determined using turnover flux calculations[21]. Mice were killed after infusion for serum, tumour, liver and kidney analysis by LC–MS. The isotope natural abundance and impurity of labelled substrate was corrected using a matrix-based algorithm. The construction of the purity matrix and C/N joint correction matrix is similar to AccuCor[39]. For calculation of the circulating amino acid concentration, the average ion counts from the *Atg7*$^{+/+}$ mice were normalized to the previously measured amino acid concentration[40]. The amino acid concentrations in the *Atg7*$^{\Delta/\Delta}$ mice were calculated proportionally.

Arginase activity assay. To follow conversion of arginine to ornithine, 15 μl serum samples were added to 5 μl of 9.7 mM $MnCl_2$, 5 μl of 360 mM pH 9.7 glycine and 5 μl of 300 μM $^{13}C_6$-arginine followed by incubation at 37 °C for 0, 5, 20, 60 or 120 min. Then, 870 μl of 40:40:20 methanol:acetonitrile:water with 0.5% formic

acid solution were added to stop the reaction; the mixture was allowed to sit on ice for 10 min. The extract was neutralized with 40 μl of 15% NH_4HCO_3 solution and centrifuged at 16,000*g* for 10 min at 4 °C. Then, 500 μl of supernatant was removed to clean tubes and stored at −80 °C until analysis by LC–MS. The LC–MS analysis was performed on the Q Exactive PLUS mass spectrometer coupled to UltiMate 3000 UHPLC system with an XBridge BEH Amide column (150 mm × 2.1 mm, 2.5 μM particle size, Waters) with the corresponding XP VanGuard Cartridge. The liquid chromatography used a 6-min isocratic elution of 28% solvent A (95%:5% H_2O:acetonitrile with 20 mM ammonium acetate, 20 mM ammonium hydroxide, pH 9.4) and 72% solvent B (20%:80% H_2O:acetonitrile with 20 mM ammonium acetate, 20 mM ammonium hydroxide, pH 9.4). The flow rate was 300 μl/min. Injection volume was 5 μl and column temperature 25 °C. The mass spectrometry scans were in negative-ion mode with a resolution of 70,000 at *m*/*z* 200. The automatic gain control target was 3×10^6 and the scan range was 75−1,000. Metabolite features were extracted in MAVEN v.707 with the labelled isotope specified and a mass accuracy window of 5 p.p.m.

Proteomic analysis by LC–MS. Technical duplicates of pooled serum samples from both $Atg7^{+/+}$ ($n = 5$) and $Atg7^{\Delta/\Delta}$ ($n = 5$) mice were processed in parallel. Two different methods were also used to reduce the amount of major serum proteins, to allow detection of rarer components: AlbuVoid (Biotech Support Group) was used to deplete albumin, and the Agilent multiple affinity removal spin cartridge mouse 3 system (Mars3) was used to remove albumin, IgG and transferrin following the manufacturer's protocol. Untreated or depleted sera were loaded onto NuPage 10% Bis-Tris Gel (Invitrogen), run a short distance into the gel, and proteins reduced, alkylated and digested with trypsin as described[41]. Digests were analysed by nano LC–MS/MS using a Dionex Ultimate 3000 RLSC nano System interfaced with Q Exactive HF (Thermofisher). Peptides were loaded onto a self-packed 100 μm × 2 cm trap (Magic C18AQ, 5 μm 200 Å, Michrom Bio resources) and washed with buffer A (0.1% trifluoroacetic acid) for 5 min with a flow rate of 10 μl/min. The trap was brought in-line with the analytical column (self-packed Magic C18AQ, 3 μm 200 Å, 75 μm × 50 cm) and fractionated at 300 nl/min using a segmented linear gradient of 4–15% B in 30 min (A: 0.2% formic acid; B: 0.16% formic acid/80% acetonitrile), 15–25%B in 40 min, 25–50% in 44 min and 50–90%B in 11 min. Mass spectrometry data were acquired using a data-dependent acquisition procedure with each cycle consisting of a MS1 scan (resolution 120,000) followed MS/MS scans (HCD relative collision energy 27%, resolution 30,000) of the 20 most intense ions using a dynamic exclusion duration of 20 s. The raw data were converted into MASCOT generic format using Proteome Discover 2.1 (Thermo Fisher) and searched against the Ensemble mouse database and a database of common laboratory contaminants (http://www.thegpm.org/crap/) using a local implementation of the global proteome machine (GPM Fury)[42]. Peptide spectrum matches were assigned to genes using BioMart Ensembl tables. To estimate differential abundances of proteins, data from all LC–MS runs were combined (neat, Albivoid-depleted and Mars3-depleted for each of the four samples). For mouse proteins with 10 or more spectral counts, differential expression was estimated using the QLSpline option of the QuasiSeq package (https://cran.r-project.org/web/packages/QuasiSeq/index.html)[43]. Data are presented as fold change (thresholded $\log_2(Atg7^{\Delta/\Delta}/Atg7^{+/+})$) with adjusted P values < 0.05. P values were adjusted using Holm correction using the 'p.adjust' function in the base R package (https://cran.r-project.org). The raw mass spectrometry data have been deposited in the MassIVE repository, entry MSV000082879.

Enzymatic assays. Levels of nitric oxide in serum were determined with the nitric oxide assay kit (ab65328, Abcam).

Histology. Mouse tissues were fixed in 10% buffer formalin solution overnight and then transferred to 70% ethanol for paraffin-embedded sections. Tissue sections were deparaffinized, rehydrated and boiled for 45 min in 10 mM pH 6 citrate buffer. Slides were blocked in 10% goat serum for an hour and then incubated at 4 °C overnight with primary antibody against Ki-67 (1:200, Ab15580, Abcam), active caspase-3 (1:300, 9661, Cell Signaling), CD3 (1:100, Ab16669, Abcam), CD4 (1:1,000, Ab183685, Abcam) and CD8 (1:100, 14-0808-82, Invitrogen). The following day, tissue sections were incubated with biotin-conjugated secondary antibody for 15 min (Vector Laboratories), 3% hydrogen peroxide for 5 min, horseradish peroxidase streptavidin for 15 min (SA-5704, Vector Laboratories) and developed by 3,3-diaminobenzidine (Vector Laboratories) followed by haematoxylin staining (3536-16, Ricca). Sections were then dehydrated, mounted in Cytoseal 60 mounting medium (8310, Thermo Scientific) and analysed using Nikon Eclipse 80i microscope. For quantification of immunhistochemistry, at least 10 images containing a minimum of 100 cells were analysed at 60× magnification for each genotype.

Western blotting. Tissues and tumour samples were grounded in liquid nitrogen, lysed in Tris lysis buffer (50 mM Tris HCl, 150 mM NaCl, 1 mM EDTA, 0.1% NP40, 5 mM $MgCl_2$, 10% glycerol), separated on 12.5% SDS–PAGE gel and then transferred on PVDF membrane (Millipore). Membranes were blocked with 5% non-fat milk for 1 h and probed overnight at 4 °C with antibodies against ASS1 (1:1,000, Ab170952, Abcam), ASL (1:500, sc-374353, Santa Cruz), OTC (1:500, sc-515791, Santa Cruz), ARG1 (1:500, sc-271430, Santa Cruz), ATG7 (1:2,000, A2856, Sigma), transferrin (1:1,000, sc-22597, Santa Cruz), ATG5 (1:1,500, Ab108327, Abcam) and β-actin (1:5,000, A1978, Sigma). Immunoreactive bands were detected using peroxidase-conjugated antibody (GE Healthcare) and enhanced chemiluminescence detection reagents (NEL105001EA, Perkin Elmer) and were analysed using the ChemiDoc XRS+ system (Biorad). Protein levels were quantified using the Image Laboratory v.6.0.1 software. Antibodies were validated with the use of positive and negative controls, following the manufacturer's protocol.

T cell depletion and flow cytometry. A week after TAM, and every 5 days, 200 μg of CD4 (clone GK1.5; BE003-1, BioXCell) and CD8 (clone 2.43; BE0061, BioXCell) antibodies were injected intraperitoneally into $Atg7^{\Delta/\Delta}$ and $Atg7^{+/+}$ mice. Two days after the first antibody injection, YUMM 1.1 (1×10^6 cells) cells were resuspended in 100 ml PBS and injected subcutaneously into the dorsal flanks of the mice. Three weeks after cell injection, mice were killed and tumours and spleen were collected. Tumours were homogenized in PBS in a gentleMACS Octo Dissociator (Miltenyi Biotec), according to the manufacturer's protocol, and passed through a 70-mm cell restrainer. Spleens were ground with a rubber grinder through steel mesh, treated with ACK Lysis Buffer to remove erythrocytes and passed through a 70-mm cell restrainer. Nonspecific binding of antibodies to cell Fc receptors was blocked using 20 ml per 10^7 cells of FcR blocker (Miltenyi Biotec). Cell surface immunostaining was performed with the following antibodies (1:200): CD11c-PE-eFluor610 (clone N418, 61-0114-82), CD4-APC (clone GK1.5, 17-0041-82) CD3-AF700 (clone 17A2, 56-0032-82) and CD11b-APC-Cy7 (clone M1/70, A15390) (eBioscience); and CD45-FITC (clone 30-F11, 103107), MHC-II-BV605 (clone M5/114.15.2, 107639), Ly6G-BV650 (clone 1A8, 127641) and CD8-BV785 (clone 53.67, 100749) (BioLegend). Aqua Live/Dead (Invitrogen) was included to determine live cells. After staining of surface markers, cells were fixed and permeabilized using transcription factor staining kit and stained with FoxP3-eFluor450 (eBioscience). Cell staining data were acquired using a LSR-II flow cytometer (BD Biosciences, BD FACS Diva v2 software) and analysed with FlowJo v.10 software (Tree Star). Live lymphocytes were gated using forward scatter area (FSC-A) versus side scatter area (SSC-A), followed by FSC-A versus forward scatter height (FSC-H), SSC-A versus side scatter height (SSC-H) plots, forward scatter width (FSC-W) versus side scatter width (SSC-W), and Aqua Live/Dead. Populations were gated as follows: CD45 (percentage $CD45^+$ of total live lymphocytes), CD3 (percentage $CD3^+$ of $CD11b^-CD11c^-CD45^+$), CD8 (percentage $CD8^+$ of CD3), CD4 (percentage $CD4^+$ of CD3), T_{reg} (percentage $FoxP3^+$ of CD4), DC (percentage $CD11c^+$ of $MHC\text{-}II^+CD45^+$) and MDSC (percentage Ly6G, $CD11b^+$ of $MHC\text{-}II^-CD45^+$).

Antibodies for western blotting, flow cytometry and immunohistochemistry were validated with the use of positive and negative controls (gene knockouts and through the use of control tissues and cell lines), and following the manufacturer's protocol.

Statistics. All statistical analyses were performed with Graphpad Prism v.7 software using two-sided Student's *t*-tests, unless specified otherwise. The sample size was chosen in advance on the basis of common practice of the described experiment and is mentioned for each experiment. No statistical methods were used to predetermine sample size. Each experiment was conducted with biological replicates and repeated multiple times. All attempts at replication were successful and no data were excluded. Mice were randomly allocated to experimental groups and the investigators were not blinded during the experiments and outcome assessment.

Reporting summary. Further information on research design is available in the Nature Research Reporting Summary linked to this paper.

Data availability

All data are available from the authors upon reasonable request. Source Data for Figs. 1d, 2b, 3d are provided with the paper. The raw mass spectrometry data have been deposited in the MassIVE repository, entry MSV000082879.

31. Ruzankina, Y. et al. Deletion of the developmentally essential gene *ATR* in adult mice leads to age-related phenotypes and stem cell loss. *Cell Stem Cell* **1**, 113–126 (2007).
32. Hara, T. et al. Suppression of basal autophagy in neural cells causes neurodegenerative disease in mice. *Nature* **441**, 885–889 (2006).
33. Meeth, K., Wang, J. X., Micevic, G., Damsky, W. & Bosenberg, M. W. The YUMM lines: a series of congenic mouse melanoma cell lines with defined genetic alterations. *Pigment Cell Melanoma Res.* **29**, 590–597 (2016).
34. Summerhayes, I. C. & Franks, L. M. Effects of donor age on neoplastic transformation of adult mouse bladder epithelium in vitro. *J. Natl. Cancer Inst.* **62**, 1017–1023 (1979).
35. Lu, W. et al. Metabolomic analysis via reversed-phase ion-pairing liquid chromatography coupled to a stand alone orbitrap mass spectrometer. *Anal. Chem.* **82**, 3212–3221 (2010).
36. Papazyan, R. et al. Physiological suppression of lipotoxic liver damage by complementary actions of HDAC3 and SCAP/SREBP. *Cell Metab.* **24**, 863–874 (2016).

37. Melamud, E., Vastag, L. & Rabinowitz, J. D. Metabolomic analysis and visualization engine for LC–MS data. *Anal. Chem.* **82**, 9818–9826 (2010).
38. Zhan, L. et al. Dysregulation of bile acid homeostasis in parenteral nutrition mouse model. *Am. J. Physiol. Gastrointest. Liver Physiol.* **310**, G93–G102 (2016).
39. Su, X., Lu, W. & Rabinowitz, J. D. Metabolite spectral accuracy on orbitraps. *Anal. Chem.* **89**, 5940–5948 (2017).
40. Sailer, M. et al. Increased plasma citrulline in mice marks diet-induced obesity and may predict the development of the metabolic syndrome. *PLoS ONE* **8**, e63950 (2013).
41. Sleat, D. E. et al. Mass spectrometry-based protein profiling to determine the cause of lysosomal storage diseases of unknown etiology. *Mol. Cell. Proteomics* **8**, 1708–1718 (2009).
42. Beavis, R. C. Using the global proteome machine for protein identification. *Methods Mol. Biol.* **328**, 217–228 (2006).
43. Lund, S. P., Nettleton, D., McCarthy, D. J. & Smyth, G. K. Detecting differential expression in RNA-sequence data using quasi-likelihood with shrunken dispersion estimates. *Stat. Appl. Genet. Mol. Biol.* **11**, 1544-6115 (2012).

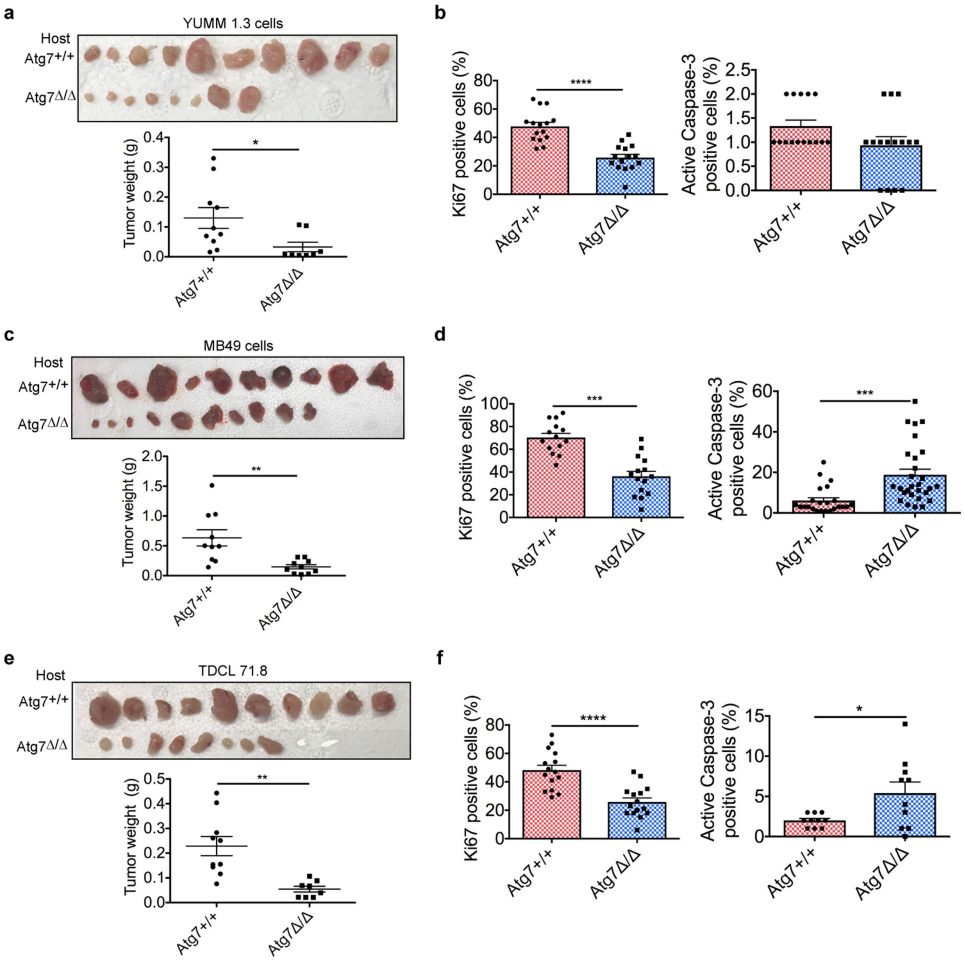

Extended Data Fig. 1 | Host autophagy promotes growth of different tumour cell types. a, **c**, **e**, Comparison of tumour weight between $Atg7^{+/+}$ ($n = 5$) and $Atg7^{\Delta/\Delta}$ (**a**, $n = 4$; **c**, $n = 5$; **e**, $n = 4$) hosts after injection of 1.3 (**a**), MB49 (**c**) or 71.8 (**e**) cells. Data are mean ± s.e.m. $^{*}P < 0.05$, $^{**}P < 0.01$. **b**, **d**, **f**, Immunohistochemistry quantification of Ki-67^{+} and active caspase-3^{+} cells in tumours from $Atg7^{+/+}$ and $Atg7^{\Delta/\Delta}$ hosts. Data are mean ± s.e.m. $^{*}P < 0.05$, $^{***}P < 0.001$, $^{****}P < 0.0001$.

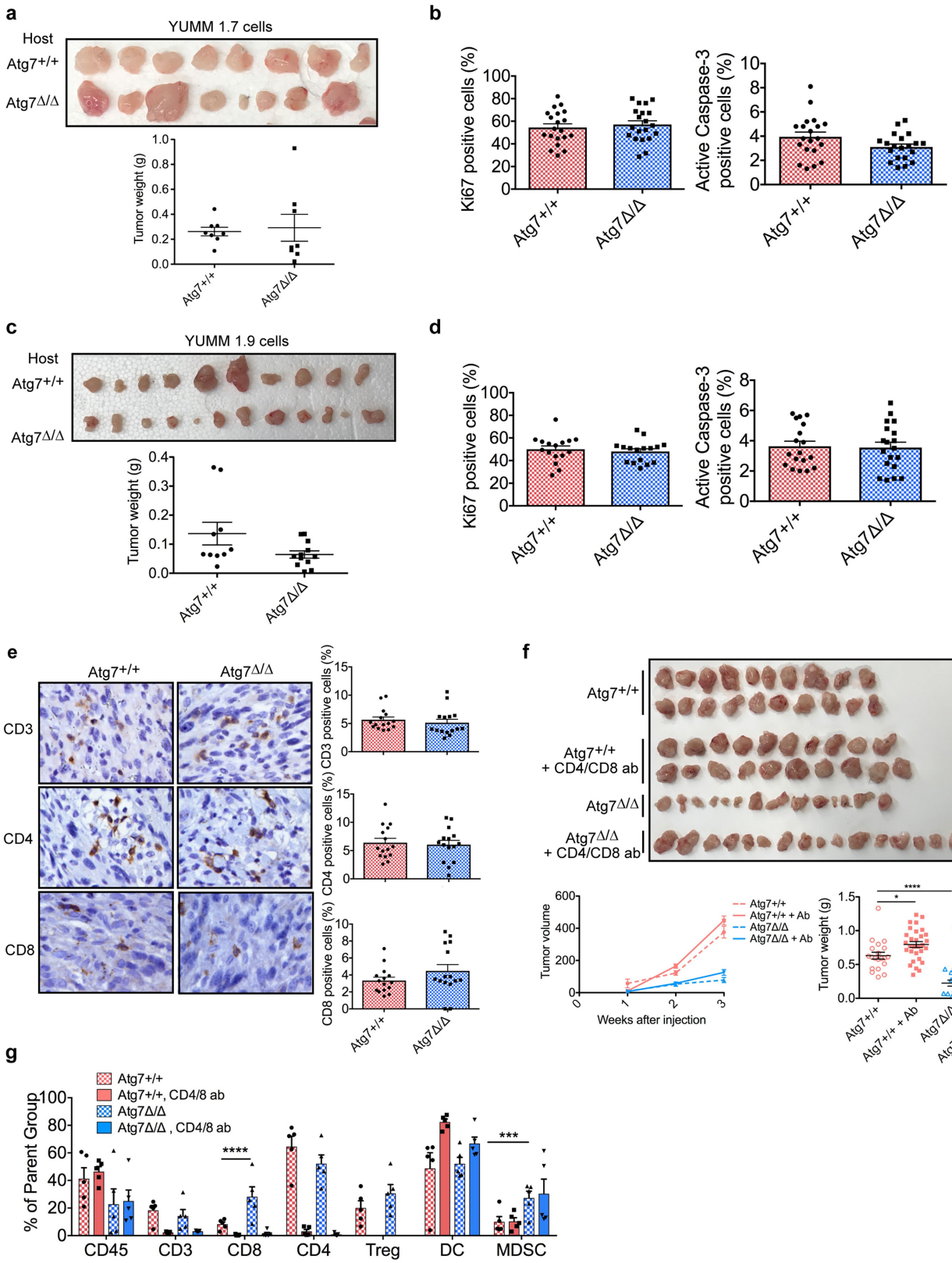

Extended Data Fig. 2 | Immune response is not involved in decreased tumour growth observed in *Atg7*$^{\Delta/\Delta}$ hosts. a, **c**, Comparison of tumour weight between *Atg7*$^{+/+}$ ($n = 5$) and *Atg7*$^{\Delta/\Delta}$ (**a**, $n = 5$; **c**, $n = 6$) hosts after injection of 1.7 (**a**) or 1.9 (**c**) cells. Data are mean ± s.e.m. **b**, **d**, Immunohistochemistry quantification of Ki-67^{+} and active caspase-3^{+} in 1.7 (**b**) and 1.9 (**d**) tumours from *Atg7*$^{+/+}$ and *Atg7*$^{\Delta/\Delta}$ hosts. Data are mean ± s.e.m. **e**, Representative immunohistochemistry images and quantification of CD3^{+}, CD4^{+} and CD8^{+} cells in tumours from *Atg7*$^{+/+}$ and *Atg7*$^{\Delta/\Delta}$ hosts. Data are mean ± s.e.m. **f**, Comparison of tumour volume and weight between *Atg7*$^{+/+}$ ($n = 10$), *Atg7*$^{+/+}$ + CD4 and CD8 antibody depletion ($n = 15$), *Atg7*$^{\Delta/\Delta}$ ($n = 7$) and *Atg7*$^{\Delta/\Delta}$ + CD4 and CD8 antibody depletion ($n = 8$) hosts. Data are mean ± s.e.m. $^{*}P < 0.05$, $^{****}P < 0.0001$. **g**, Fold change in immune components between *Atg7*$^{+/+}$ and *Atg7*$^{\Delta/\Delta}$, with or without antibody depletion ($n = 5$ each). T_{reg}, T regulatory cells; DC, dendritic cells; MDSC, myeloid-derived suppressor cells. Data are mean ± s.e.m. $^{***}P < 0.001$, $^{****}P < 0.0001$, by two-way ANOVA test.

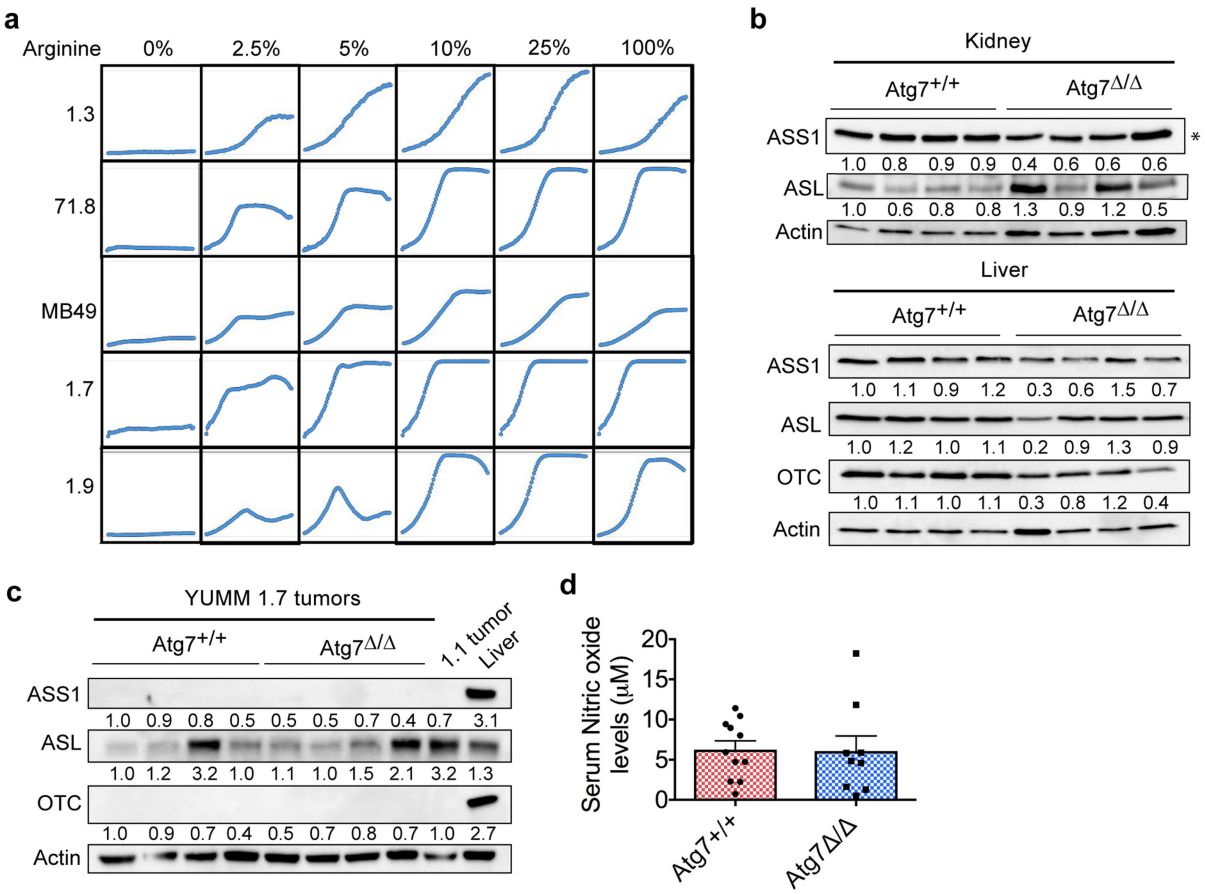

Extended Data Fig. 3 | Tumour cells are arginine auxotrophs. **a**, YUMM 1.3, 71.8, MB49 and YUMM 1.7, 1.9 proliferation in vitro, in medium containing different percentages of arginine. Cell density was measured every 2 h using the IncuCyte. Data are representative of three independent experiments performed in duplicate. **b**, Western blotting showing expression of ASS1, ASL and OTC in kidneys and livers from $Atg7^{+/+}$ and $Atg7^{\Delta/\Delta}$ hosts. $^{*}P < 0.05$ compared to $Atg7^{+/+}$ hosts. Data are representative of three independent experiments. Actin was used as a loading (kidney ASL and liver OTC) and processing (kidney ASS1, liver ASS1 and ASL) control. **c**, Western blotting showing expression of ASS1, ASL and OTC in YUMM 1.7 tumours from $Atg7^{+/+}$ and $Atg7^{\Delta/\Delta}$ hosts. Data are representative of two independent experiments. Actin was used as a loading (OTC) and processing (ASS1 and ASL) control. **d**, Analysis of levels of nitric oxide in serum in $Atg7^{+/+}$ ($n = 11$) and $Atg7^{\Delta/\Delta}$ ($n = 9$) hosts. Data are mean ± s.e.m.

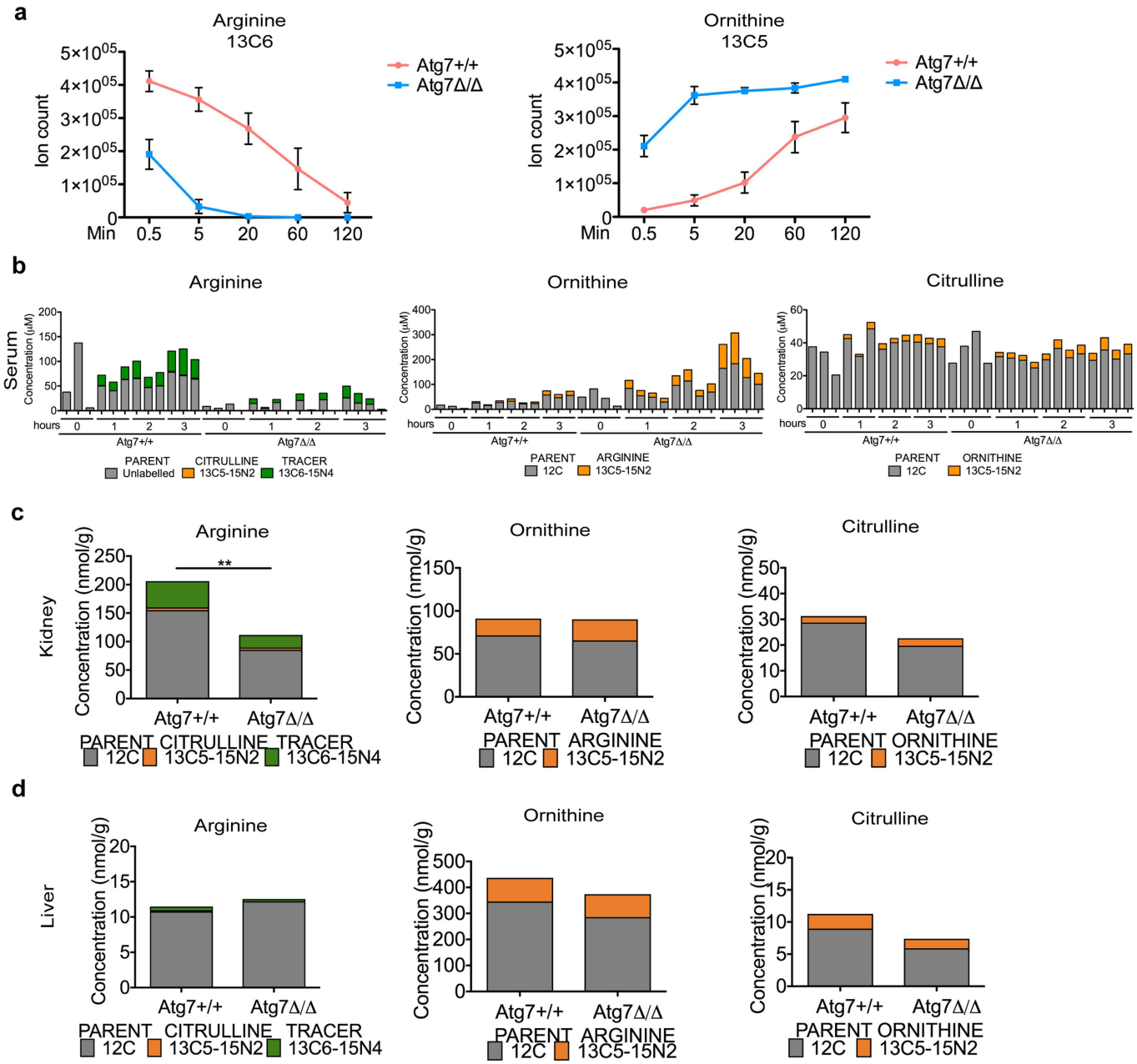

Extended Data Fig. 4 | *Atg7* deletion increases serum arginine degradation but does not modify arginine metabolism in kidney and liver. a, Serum $^{13}C_6$-arginine and $^{13}C_5$-ornithine in $Atg7^{+/+}$ and $Atg7^{\Delta/\Delta}$ hosts ($n = 3$ each) over time. Data are mean ± s.e.m. **b**, Concentration (in μM) of arginine, citrulline and ornithine in serum from $Atg7^{+/+}$ ($n = 3$) and $Atg7^{\Delta/\Delta}$ hosts ($n = 4$), after infusion with $^{13}C_6{}^{15}N_4$-arginine. **c**, **d**, Concentration (in nmol g^{-1}) of arginine, citrulline and ornithine in kidneys (**c**) and livers (**d**) from $Atg7^{+/+}$ and $Atg7^{\Delta/\Delta}$ hosts ($n = 2$ each) after infusion with $^{13}C_6{}^{15}N_4$-arginine. Data are mean. $^{**}P < 0.01$ by two-way ANOVA test.

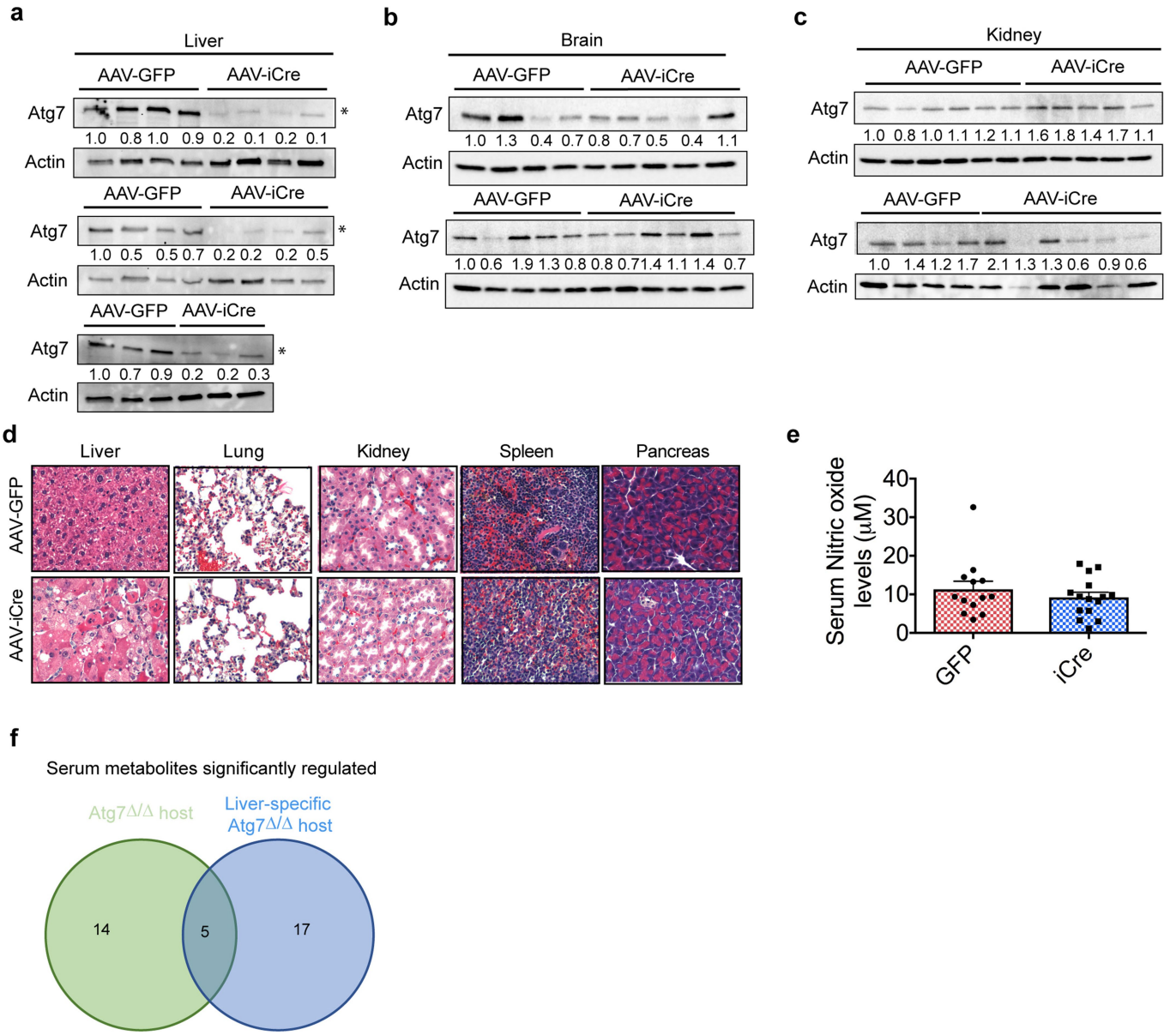

Extended Data Fig. 5 | Liver-specific deletion of *Atg7* leads to liver-cell enlargement without affecting other tissues. a–**c**, Western blotting showing expression of *Atg7* in livers ($n = 11$ each) (**a**), brains ($n = 9$ and 11, respectively) (**b**) and kidneys ($n = 10$ each) (**c**) from $Atg7^{+/+}$ hosts and hosts with liver-specific deletion of *Atg7*. *$P < 0.05$ compared to $Atg7^{+/+}$ hosts. Data are representative of two independent experiments. Actin was used as a loading control. **d**, Representative haematoxylin and eosin tissue staining from $Atg7^{+/+}$ hosts and hosts with liver-specific deletion of *Atg7*. Images are representative of two independent experiments. **e**, Analysis of levels of nitric oxide in serum, in $Atg7^{+/+}$ hosts ($n = 13$) and hosts with liver-specific deletion of *Atg7* ($n = 15$). Data are mean ± s.e.m. **f**, Comparison of serum metabolites that are significantly regulated in $Atg7^{\Delta/\Delta}$ hosts and hosts with liver-specific deletion of *Atg7* ($n = 17$ each, $P < 0.05$).

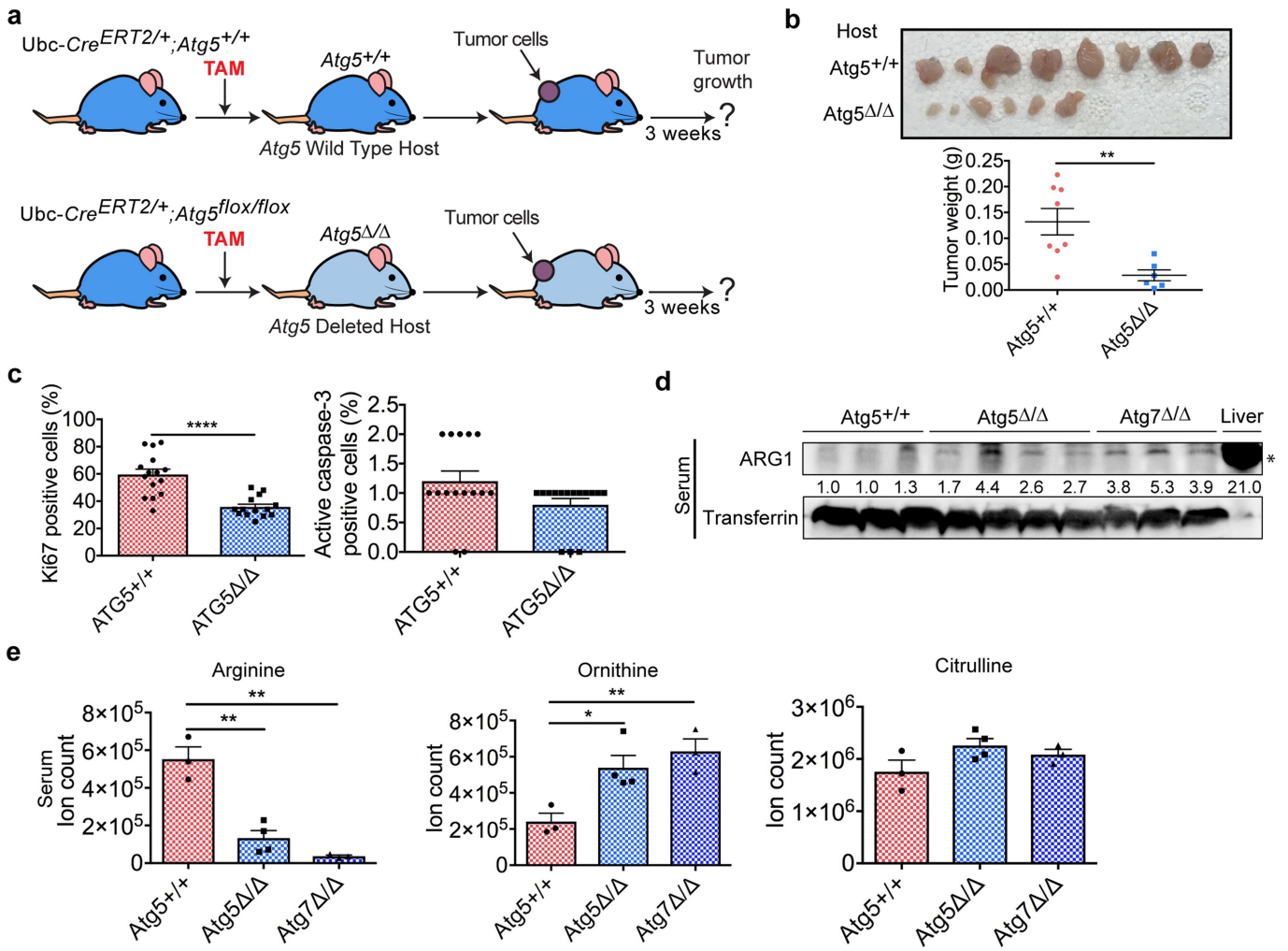

Extended Data Fig. 6 | *Atg5* deletion increased serum ARG1, decreased serum arginine and tumour growth. a, Experimental design to induce host mice with conditional whole-body deletion of *Atg5* ($Atg5^{\Delta/\Delta}$) and wild-type controls ($Atg5^{+/+}$) with which to assess tumour growth. *Ubc-cre*$^{ERT2/+}$;$Atg5^{+/+}$ and *Ubc-cre*$^{ERT2/+}$;$Atg5^{flox/flox}$ mice were injected with TAM at 8 to 10 weeks of age to delete *Atg5* and create $Atg5^{+/+}$ and $Atg5^{\Delta/\Delta}$ hosts. Mice were then injected subcutaneously with tumour cells and tumour growth was monitored over three weeks. **b**, Comparison of tumour weight between $Atg5^{+/+}$ ($n=4$) and $Atg5^{\Delta/\Delta}$ ($n=3$) hosts. Data are mean ± s.e.m. $^{**}P<0.01$. **c**, Immunohistochemistry quantification of Ki-67$^+$ and active caspase-3$^+$ cells in tumours from $Atg5^{+/+}$ and $Atg5^{\Delta/\Delta}$ hosts. Data are mean ± s.e.m. $^{****}P<0.0001$. **d**, Western blotting showing expression of ARG1 in serum from $Atg5^{+/+}$ ($n=3$), $Atg5^{\Delta/\Delta}$ ($n=4$) and $Atg7^{\Delta/\Delta}$ ($n=3$) hosts. $^{*}P<0.05$ compared to $Atg5^{+/+}$ hosts. Transferrin was used as a loading control. **e**, Levels of arginine, ornithine and citrulline in serum in $Atg5^{+/+}$ ($n=4$) and $Atg5^{\Delta/\Delta}$ ($n=3$) hosts, obtained by LC–MS. Data are mean ± s.e.m. $^{*}P<0.05$, $^{**}P<0.01$.

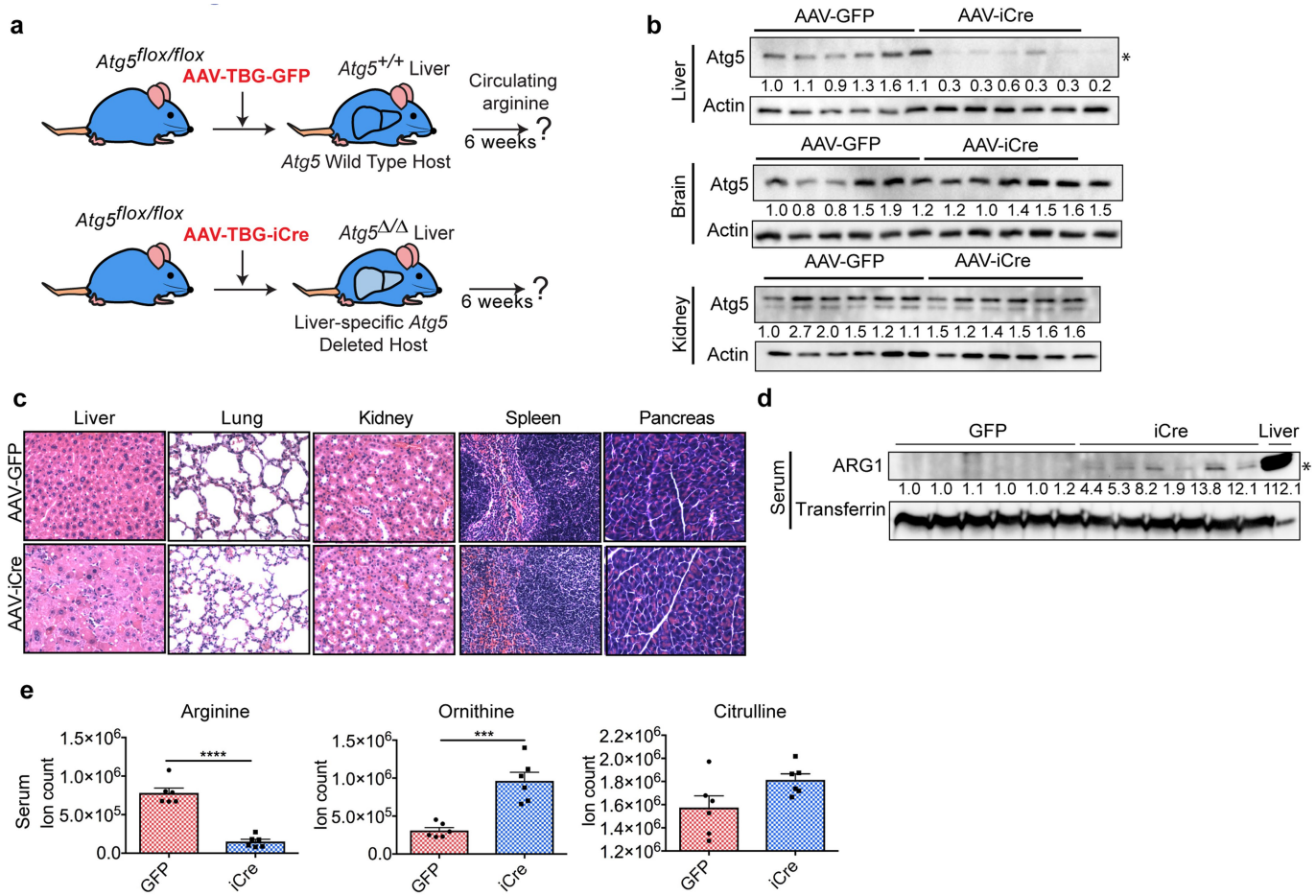

Extended Data Fig. 7 | Liver-specific *Atg5*-deleted hosts present liver-cell enlargement, increased serum ARG1 and decreased serum arginine. a, Experimental design to induce liver-specific deletion of *Atg5*. $Atg5^{flox/flox}$ mice were injected in the tail vein with AAV–TBG–GFP or AAV–TBG–iCre at 8 to 10 weeks of age to delete *Atg5* in the liver and create $Atg5^{+/+}$ hosts and hosts with liver-specific deletion of *Atg5*, respectively. **b**, Western blotting showing expression of *Atg5* in the livers, brains and kidneys of $Atg5^{+/+}$ hosts and hosts with liver-specific deletion of *Atg5* ($n = 6$ each). $^*P < 0.05$ compared to $Atg5^{+/+}$ hosts. Actin was used as a loading control **c**, Haematoxylin and eosin tissue staining from $Atg5^{+/+}$ hosts and hosts with liver-specific deletion of *Atg5* ($n = 6$ each). **d**, Western blotting showing expression of ARG1 in serum from $Atg5^{+/+}$ hosts and hosts with liver-specific deletion of *Atg5* ($n = 6$ each). $^*P < 0.05$ compared to $Atg5^{+/+}$ hosts. Transferrin was used as a loading control. **e**, Levels of arginine, ornithine and citrulline in serum in $Atg5^{+/+}$ hosts and hosts with liver-specific deletion of *Atg5* ($n = 6$ each), obtained by LC–MS. Data are mean ± s.e.m. $^{***}P < 0.001$, $^{****}P < 0.0001$.

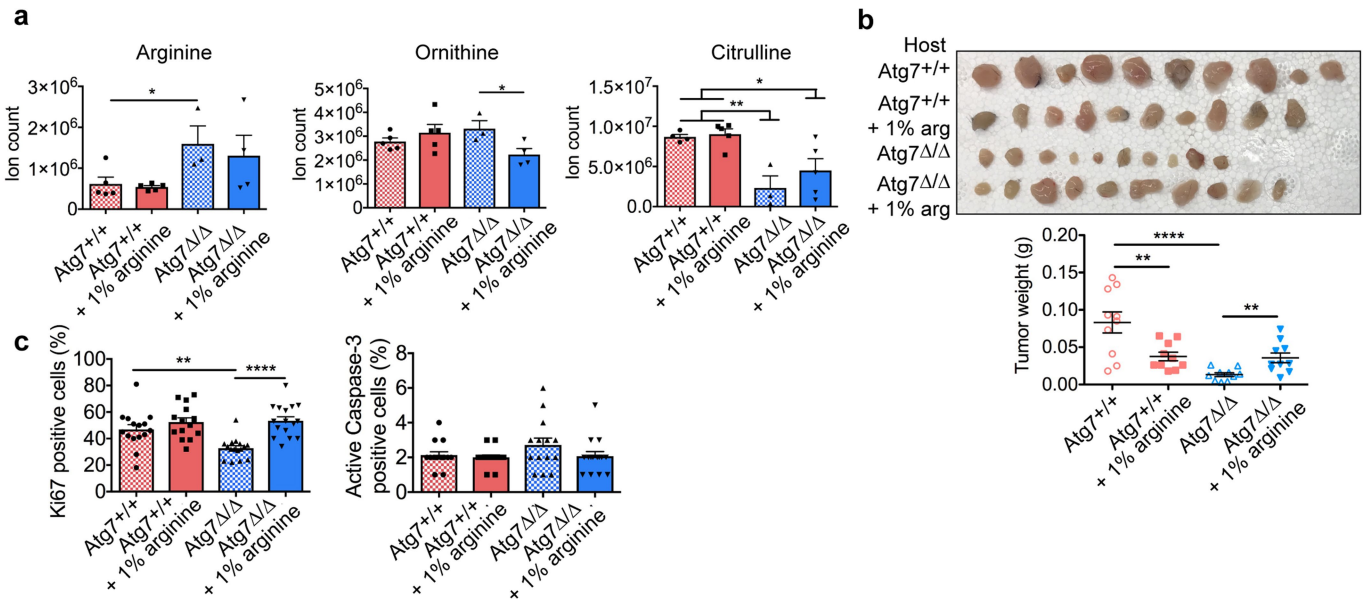

Extended Data Fig. 8 | Dietary arginine supplementation rescues YUMM 1.3 tumour growth in *Atg7*$^{\Delta/\Delta}$ hosts. a, Serum arginine, ornithine and citrulline in *Atg7*$^{+/+}$ ($n = 5$), *Atg7*$^{+/+}$ + 1% arginine ($n = 5$), *Atg7*$^{\Delta/\Delta}$ ($n = 6$) and *Atg7*$^{\Delta/\Delta}$ + 1% arginine ($n = 6$) hosts, obtained by LC–MS. Data are mean ± s.e.m. $^{*}P < 0.05$, $^{**}P < 0.01$. **b**, Comparison of YUMM 1.3 tumour weight between *Atg7*$^{+/+}$ and *Atg7*$^{\Delta/\Delta}$ ($n = 5$ each) hosts, with or without arginine supplementation. Data are mean ± s.e.m. $^{**}P < 0.01$, $^{****}P < 0.0001$. **c**, Immunohistochemistry quantification of Ki-67^{+} and active caspase-3^{+} cells in tumours from *Atg7*$^{+/+}$ and *Atg7*$^{\Delta/\Delta}$ hosts, with or without arginine supplementation. Data are mean ± s.e.m. $^{**}P < 0.01$, $^{****}P < 0.0001$.

nature research

Corresponding author(s): Eileen White

Reporting Summary

Nature Research wishes to improve the reproducibility of the work that we publish. This form provides structure for consistency and transparency in reporting. For further information on Nature Research policies, see Authors & Referees and the Editorial Policy Checklist.

Statistical parameters

When statistical analyses are reported, confirm that the following items are present in the relevant location (e.g. figure legend, table legend, main text, or Methods section).

n/a	Confirmed	
☐	☒	The exact sample size (*n*) for each experimental group/condition, given as a discrete number and unit of measurement
☐	☒	An indication of whether measurements were taken from distinct samples or whether the same sample was measured repeatedly
☐	☒	The statistical test(s) used AND whether they are one- or two-sided *Only common tests should be described solely by name; describe more complex techniques in the Methods section.*
☒	☐	A description of all covariates tested
☒	☐	A description of any assumptions or corrections, such as tests of normality and adjustment for multiple comparisons
☐	☒	A full description of the statistics including central tendency (e.g. means) or other basic estimates (e.g. regression coefficient) AND variation (e.g. standard deviation) or associated estimates of uncertainty (e.g. confidence intervals)
☐	☒	For null hypothesis testing, the test statistic (e.g. *F*, *t*, *r*) with confidence intervals, effect sizes, degrees of freedom and *P* value noted *Give P values as exact values whenever suitable.*
☒	☐	For Bayesian analysis, information on the choice of priors and Markov chain Monte Carlo settings
☒	☐	For hierarchical and complex designs, identification of the appropriate level for tests and full reporting of outcomes
☒	☐	Estimates of effect sizes (e.g. Cohen's *d*, Pearson's *r*), indicating how they were calculated
☐	☒	Clearly defined error bars *State explicitly what error bars represent (e.g. SD, SE, CI)*

Our web collection on statistics for biologists may be useful.

Software and code

Policy information about availability of computer code

Data collection	BD FACS Diva v2
Data analysis	Prism v7, Maven v707, Image Lab v6.0.1, FlowJo v10

For manuscripts utilizing custom algorithms or software that are central to the research but not yet described in published literature, software must be made available to editors/reviewers upon request. We strongly encourage code deposition in a community repository (e.g. GitHub). See the Nature Research guidelines for submitting code & software for further information.

Data

Policy information about availability of data

All manuscripts must include a data availability statement. This statement should provide the following information, where applicable:

- Accession codes, unique identifiers, or web links for publicly available datasets
- A list of figures that have associated raw data
- A description of any restrictions on data availability

All data are available from the corresponding authors upon reasonable request.

Field-specific reporting

Please select the best fit for your research. If you are not sure, read the appropriate sections before making your selection.

☒ Life sciences ☐ Behavioural & social sciences ☐ Ecological, evolutionary & environmental sciences

For a reference copy of the document with all sections, see nature.com/authors/policies/ReportingSummary-flat.pdf

Life sciences study design

All studies must disclose on these points even when the disclosure is negative.

Sample size	The sample size was chosen in advance on the basis of common practice of the described experiment and is mentioned for each experiment. No statistical methods were used to predetermine sample size.
Data exclusions	No data were excluded
Replication	Each experiment was conducted with biological replicates and repeated multiple times. All attempts at replication were successful.
Randomization	Mice were randomly allocated to experimental groups.
Blinding	The investigators were not blinded during the experiments and outcome assessment.

Reporting for specific materials, systems and methods

Materials & experimental systems

n/a	Involved in the study
☒	☐ Unique biological materials
☐	☒ Antibodies
☐	☒ Eukaryotic cell lines
☒	☐ Palaeontology
☐	☒ Animals and other organisms
☒	☐ Human research participants

Methods

n/a	Involved in the study
☒	☐ ChIP-seq
☒	☐ Flow cytometry
☒	☐ MRI-based neuroimaging

Antibodies

Antibodies used	For immunohistochemistry : Ki67 (1:200, Ab15580, Abcam), active Caspase-3 (1:300, #9661, Cell Signaling), CD3 (1:100, Ab16669, Abcam), CD4 (1:1,000, Ab183685, Abcam) and CD8 (1:100, 14-0808-82, Invitrogen). For western blotting: ASS1 (1:1,000 , Ab170952, Abcam), ASL (1:500, sc-374353, Santa Cruz), OTC (1:500, sc-515791, Santa Cruz), ARG1 (1:500, sc-271430, Santa Cruz), ATG7 (1:2,000, A2856, Sigma), transferrin (1:1,000, sc-22597, Santa Cruz), ATG5 (1:1,500, Ab108327, Abcam) and β-actin (1:5,000, A1978, Sigma). For antibody depletion: 200 ug of CD4 (clone GK1.5; BE003-1, BioXCell) and CD8 (clone 2.43; BE0061, BioXCell). For flow cytometry (1:200), the following antibodies purchased from eBioscience: CD11c-PE-eFluor610 (clone N418, 61-0114-82), CD4-APC (clone GK1.5, 17-0041-82) CD3-AF700 (clone 17A2, 56-0032-82), CD11b-APC-Cy7 (clone M1/70, A15390); and the following antibodies from BioLegend: CD45-FITC (clone 30-F11, 103107), MHC-II-BV605 (clone M5/114.15.2, 107639), Ly6G-BV650 (clone 1A8, 127641), CD8-BV785 (clone 53.67, 100749).
Validation	Antibodies for western blotting, flow cytometry and immunohistochemistry were validated with the use of positive and negative control (gene knock outs and through the use of control tissues and cell lines) and following manufacturer's protocol.

Eukaryotic cell lines

Policy information about cell lines

Cell line source(s)	YUMM 1.1, 1.3, 1.7 and 1.9 cells derived from BrafV600E/+, Pten-/-, Cdkn2-/- C57Bl/6J mouse melanomas and were generated previously in the Bosenberg laboratory. Mouse lung cancer cell line 71.8 was derived from p53-/-, KrasG12D/+ mouse lung tumors previously in our laboratory and the MB49 cell line was provided by the Ratliff laboratory.
Authentication	YUMM 1.1, 1.3, 1.7, 1.9, 71.8 and MB49 were authenticated using whole exome sequencing.

Mycoplasma contamination	Cells were tested negative for mycoplasma contamination
Commonly misidentified lines (See ICLAC register)	No misidentifed lines were used

Animals and other organisms

Policy information about studies involving animals; ARRIVE guidelines recommended for reporting animal research

Laboratory animals	For whole-body Atg7 deletion : 8 to 10 weeks old C57Bl/6J Ubc-CreERT2/+;Atg7flox/flox and Ubc-CreERT2/+;Atg7+/+ male mice ; For liver-specific Atg7 deletion : 8 to 10 weeks old C57Bl/6J Atg7flox/flox male mice For whole-body Atg5 deletion : 8 to 10 weeks old C57Bl/6J Ubc-CreERT2/+;Atg5flox/flox and Ubc-CreERT2/+;Atg5+/+ male mice ; For liver-specific Atg5 deletion : 8 to 10 weeks old C57Bl/6J Atg5flox/flox male mice
Wild animals	The study did not involve wild animals
Field-collected samples	The study did not involve samples collected from the field.